Relative terrestrial exposure ages inferred from meteoric ^{10}Be and NO_3^- concentrations in soils along the Shackleton Glacier, Antarctica

Melisa A. Diaz[1,2†], Lee B. Corbett[3], Paul R. Bierman[3], Byron J. Adams[4], Diana H. Wall[5], Ian D. Hogg[6,7], Noah Fierer[8], W. Berry Lyons[1,2]

[1]School of Earth Sciences, The Ohio State University, Columbus, OH, 43210, USA
[2]Byrd Polar and Climate Research Center, The Ohio State University, Columbus, OH, 43210, USA
[3]Department of Geology, University of Vermont, Burlington, VT, 05405, USA
[4]Department of Biology, Evolutionary Ecology Laboratories, and Monte L. Bean Museum, Brigham Young University, Provo, UT, 84602, USA
[5]Department of Biology and School of Global Environmental Sustainability, Colorado State University, Fort Collins, CO, 80523, USA
[6]Canadian High Arctic Research Station, Polar Knowledge Canada, Cambridge Bay, NU, X0B0C0, Canada
[7]School of Science, University of Waikato, Hamilton, 3216, New Zealand
[8]Department of Ecology and Evolutionary Biology and Cooperative Institute for Research in Environmental Science, University of Colorado Boulder, Boulder, CO, 80309, USA
[†]Now at Geology and Geophysics, and Applied Ocean and Physics and Engineering, Woods Hole Oceanographic Institution, Woods Hole, MA, 02543, USA

Correspondence to: Melisa A. Diaz (diaz.237@osu.edu)

Abstract. Modeling studies and field mapping show that increases in ice thickness during glacial periods were not uniform across Antarctica. Rather, outlet glaciers that flow through the Transantarctic Mountains (TAM) experienced the greatest changes in ice thickness. As a result, ice-free areas that are currently exposed may have been covered by ice at various points during the Cenozoic, complicating the understanding of ecological succession in TAM soils. We collected soil surface samples and depth profiles every 5 cm to refusal (up to 30 cm) from eleven ice-free areas along the Shackleton Glacier, a major outlet glacier of the East Antarctic Ice Sheet (EAIS). We measured meteoric ^{10}Be and NO_3^- concentrations to calculate measured (using ^{10}Be inventory), estimated (using NO_3^-), and inferred (using surface ^{10}Be concentration) surface exposure ages, both with and without assuming erosion. Exposure ages ranged from 58 ka to >6.5 Ma correcting for erosion and 57 ka to 1.9 Ma without erosion, with the youngest ages near the glacier terminus and at lower relatively elevations. We correlated NO_3^- concentrations with meteoric ^{10}Be concentrations to estimate exposure ages for all locations with NO_3^- depth profiles but only surface ^{10}Be data. Our results indicated that NO_3^- concentrations can be used in conjunction with few meteoric ^{10}Be data to rapidly and efficiently estimate relative surface exposure ages. In comparing NO_3^- and ^{10}Be depth profile measurements, we find that much of the southern portion of the Shackleton Glacier region has likely developed undisturbed under a hyper-arid climate regime.

1. Introduction

One of the most intriguing questions in biogeography concerns the relationship between the evolution of terrestrial organisms and landscape disturbance (e.g. glacial overriding), particularly in Antarctica. Current data indicate that organism lineages have survived in some Antarctic soils for possibly millions of years, despite multiple glaciations throughout the Pleistocene (Convey et al., 2008; Fraser et al., 2012; Stevens and Hogg, 2003). It is still unclear how and where these organisms found suitable glacial refugia given the high salt concentrations in high-elevation soils (Lyons et al., 2016). The most biodiverse soils in the Ross Sea sector are at low elevations near the coast, where the Ross Ice Shelf or sea ice meet the Transantarctic Mountains (TAM) (Collins et al., 2020). These soils are also those which are most susceptible to glacial overriding during glacial maxima, though the timing of retreat and glacial extent is still unknown on local scales (Golledge et al., 2012; MacKintosh et al., 2011).

Antarctica is believed to have maintained a persistent ice sheet since at least the Eocene epoch, and the East and West Antarctic Ice Sheets (EAIS and WAIS, respectively) have waxed and waned since at least the Miocene (Gasson et al., 2016; Gulick et al., 2017). Sediment core records collected from the Ross Sea and ice cores from the Antarctic interior indicate that the EAIS and WAIS have undergone dozens of glacial and interglacial cycles throughout the Cenozoic (Augustin et al., 2004; Talarico et al., 2012). The WAIS is a marine-terminating ice sheet with a grounding line below sea level, which decreases the stability of the ice sheet and results in rapid ice sheet advance and retreat during glacial periods compared to the EAIS (Pollard and DeConto, 2009). The EAIS is grounded above sea level and is generally more stable than the WAIS. The EAIS and WAIS were at their most recent greatest extent during the Last Glacial Maximum (LGM) (~22,000 yrs. ago) (Clark et al., 2009). During the LGM, the EAIS expanded along its margins and the greatest increases in height occurred at outlet glaciers, which flow through exposed peaks of the TAM and drain into the Ross and Weddell Seas (Anderson et al., 2002; Golledge et al., 2012; Mackintosh et al., 2014). As a result, many of the currently exposed TAM soils were overrun by ice during the LGM and some may have only recently been exposed.

Much of the Antarctic continent is a polar desert and geomorphological data from ice-free soils in the McMurdo Dry Valleys indicate that some regions have likely been hyper-arid for as long as 15 Ma (Marchant et al., 1996; Valletta et al., 2015). As such, atmospherically-derived constituents, including salts and metals, can accumulate in exposed Antarctic

soils at concentrations similar to those from the Atacama and Namib Deserts (Diaz et al., 2020; Lyons et al., 2016; Reich and Bao, 2018). Using soil nitrate concentrations from the Meyer Desert in the Beardmore Glacier region and nitrate fluxes calculated from a Dominion Range ice core, Lyons et al. (2016) estimated that at least 750,000 years have passed since the Meyer Desert had wide-spread soil wetting. It is likely that other high elevation and inland locations in the TAM also have high concentrations of salts and similarly old "wetting ages".

We calculated relative surface soil exposure ages of ice-free areas along the Shackleton Glacier, a major outlet glacier of the EAIS. Outlet glaciers are among the most sensitive areas to glaciological change in Antarctica, and changes in their extents over time are recorded in nearby sedimentary deposits (Golledge et al., 2013; Jones et al., 2015; Scherer et al., 2016; Spector et al., 2017). The Shackleton Glacier flows between several exposed peaks of the Central Transantarctic Mountains (CTAM) and ice-free areas are present at both low and high elevations. We report concentrations of meteoric ^{10}Be and nitrate (NO_3^-) in soils from eleven distinct ice-free areas and use these data to estimate the exposure ages using different assumptions. The sampling methodology was designed to capture soils which have low salt concentrations due to recent exposure from glacial retreat following the LGM and soils that were exposed since at least the last glacial period. These age data are among few surface exposure ages in the CTAM (Ackert and Kurz, 2004; Balter-Kennedy et al., 2020), are the only age estimates of soils from the Shackleton Glacier region, inform how the EAIS responds to changes in climate, and are crucial in understanding Antarctic terrestrial biogeography.

2. Background

2.1. Cosmogenic nuclide exposure age dating and meteoric ^{10}Be systematics

^{10}Be is a cosmogenic radionuclide with a half-life of 1.39 Ma (Korschinek et al., 2010) that is produced both in the atmosphere (meteoric) and *in-situ* in mineral grains. In the atmosphere, N and O gases are bombarded by high energy cosmic radiation to produce meteoric ^{10}Be. Particle reactive ^{10}BeO or $^{10}Be(OH)_2$ is produced and removed from the atmosphere by wet and dry deposition (McHargue and Damon, 1991). At Earth's surface, meteoric ^{10}Be sorbs onto clay particles and it is insoluble in most natural waters of pH greater than 4 (Brown et al., 1992; You et al., 1989). The clay particles can be redistributed to lower depths in the soil profile due to particle migration or can be transported by winds. As such, the total

number of ^{10}Be atoms in a soil profile, its inventory, is a function of surface exposure duration, erosion, clay particle translocation, solubility, and sedimentation. If delivery rates can be estimated, meteoric ^{10}Be can be used as a tool to understand exposure age, erosion rates, and soil residence times (see Willenbring and Von Blanckenburg, 2009 and references within).

The measurement meteoric ^{10}Be in soil has enabled researchers to date surfaces and features in Antarctica. Previous studies have measured meteoric ^{10}Be in the McMurdo Dry Valleys (MDV) and Victoria Land soils and sediments to calculate exposure ages and to determine the onset of the current polar desert regime (Dickinson et al., 2012a; Graham et al., 2002; Schiller et al., 2009; Valletta et al., 2015). In general, these previous studies found that high elevation, northern fringe regions along the Ross Embayment have been hyper-arid since at least the Pliocene. Meteoric ^{10}Be data have yet to be published from the CTAM which represent ice sheet dynamics and climatic conditions closer to the Polar Plateau.

2.2. Nitrate systematics in Antarctic soils

The nitrogen cycle in Antarctica differs greatly from the nitrogen cycle in temperate regions, primarily due to scarce biomass and vascular plants (Cary et al., 2010; Michalski et al., 2005). Nitrogen in CTAM soils primarily exists as nitrate (NO_3^-) and is primarily sourced from the atmosphere, with varying contributions from the troposphere and stratosphere (Diaz et al., 2020; Lyons et al., 2016; Michalski et al., 2005). Similar to meteoric ^{10}Be, NO_3^- is deposited on exposed soils, though in contrast to ^{10}Be, nitrate salts are highly water-soluble. Once deposited on the surface, nitrate salts can be dissolved and transported to lower elevations or eluted to depth when wetted (i.e. during ice/snow melt events). However, the hyper-arid climate of the CTAM allows NO_3^- to accumulate at high concentrations in soils (Claridge and Campbell, 1968a; Diaz et al., 2020; Lyons et al., 2016). Soil NO_3^- concentrations have the potential to inform wetting history and possibly glacial history in the CTAM due to the relatively high solubility of nitrate salts, though uncertainties regarding heterogeneous deposition and post-depositional alteration (such as re-volatilization and photolysis) require further investigation (Diaz et al., 2020; Frey et al., 2009; Graham et al., 2002).

2.3. Relative exposure age dating approach

Here, we used meteoric ^{10}Be and NO_3^- concentrations to estimate CTAM relative exposure ages, acknowledging the widespread use of *in-situ* exposure age dating which we later use for cross-validation. *In-situ* cosmogenic nuclides, such as ^{10}Be, ^{26}Al, ^{21}Ne, and ^{3}He, have been measured to determine surface exposure ages at several locations across Antarctica, particularly in the MDV and other exposed surfaces in Victoria Land (e.g. Balco et al., 2019; Brook et al., 1993, 1995; Bruno et al., 1997; Ivy-Ochs et al., 1995; Strasky et al., 2009). There are considerably fewer studies from the CTAM (Ackert and Kurz, 2004; Balter-Kennedy et al., 2020; Bromley et al., 2010; Kaplan et al., 2017; Spector et al., 2017), and previously reported exposure ages of CTAM moraines and boulders from these studies ranged from <10 ka to >14 Ma. We seek to utilize NO_3^- and meteoric ^{10}Be concentrations to attain a greater number of surface exposure ages and understand the relationship between NO_3^- and ^{10}Be in the hyper-arid environment of the CTAM. Exposure ages are determined by three approaches: "measured" by using measured meteoric ^{10}Be concentrations in depth profiles, "estimated" by using NO_3^- concentrations to estimate ^{10}Be concentrations, and "inferred" by using the maximum/surface concentration of ^{10}Be in the soil profile to infer the total number of ^{10}Be atoms in the profile (Graly et al., 2010). These approaches are described in Sections 4.3 and 5.3.

3. Study sites

Shackleton Glacier (~84.5 to 86.4°S; ~130 km long and ~10 km wide) is a major outlet glacier of the EAIS that drains north into the Ross Embayment with other CTAM outlet glaciers to form the Ross Ice Shelf (RIS) (Fig. 1). The ice flows between exposed surfaces of the Queen Maud Mountains, which range from elevations of ~150 m near the RIS to >3,500 m further inland. The basement geology of the Shackleton Glacier region is comprised of igneous and metamorphic rocks that formed from intruded and metamorphosed sedimentary and volcanic strata during the Ross Orogeny (450-520 Ma) (Elliot and Fanning, 2008). The southern portion of the region consists of the Devonian-Triassic Beacon Supergroup and the Jurassic Ferrar Group, while the northern portions consists of Pre-Devonian granitoids and the Early to Mid-Cambrian Taylor Group (Elliot and Fanning, 2008; Paulsen et al., 2004). These rocks serve as primary parent material for soil formation (Claridge and Campbell, 1968b). Deposits of the Sirius Group, the center of the stable vs. dynamic EAIS debate, have been previously identified in the southern portion of the Shackleton Glacier region, particularly at Roberts Massif (Fig. 2) and Bennett Platform, with a small exposure at Schroeder Hill (Hambrey et al., 2003).

The valleys and other ice-free areas within the region have been modified by the advance and retreat of the Shackleton Glacier, smaller tributary glaciers, and alpine glaciers. Similar to the Beardmore Glacier region, the Shackleton Glacier region is a polar desert, which results in the high accumulation of salts in soils. The surface is comprised primarily of till, weathered primary bedrock, and scree, which ranges in size from small boulders and cobbles to sand and silt. Clay minerals have been previously identified in all samples from Roberts Massif and are likely ubiquitous throughout the region (Claridge and Campbell, 1968b). However, the clays are a mixture of those derived from sedimentary rocks and contemporaneous weathering (Claridge and Campbell, 1968b). Thin, boulder belt moraines, characteristic of cold-based glaciers, were deposited over bedrock and tills at Roberts Massif, while large moraines were deposited at Bennett Platform (Fig. 2; Balter-Kennedy et al., 2020; Claridge and Campbell, 1968). Additional information on the sample locations and surface features is provided in Tables 1 and 2.

4. Methods

4.1. Sample collection

During the 2017-2018 austral summer, we visited eleven ice-free areas along the Shackleton Glacier: Roberts Massif, Schroeder Hill, Bennett Platform, Mt. Augustana, Mt. Heekin, Thanksgiving Valley, Taylor Nunatak, Mt. Franke, Mt. Wasko, Nilsen Peak, and Mt. Speed (Fig. 1). These areas represent soils from near the head of the glacier to near the glacier terminus at the coast of the RIS. Two surface samples (Table 1) were collected at each location (except for Nilsen Peak and Mt. Wasko, represented by only one sample) with a plastic scoop and stored in Whirl-Pak™ bags. One sample was collected furthest from the Shackleton Glacier or other tributary glaciers (within ~2,000 m) to represent soils that were likely exposed during the LGM and previous recent glacial periods. A second sample was collected closer to the glacier (between ~1,500 and 200 m from the first sample) to represent soils likely to have been exposed by more recent ice margin retreat.

Soil pits were dug by hand at the sampling locations furthest from the glacier for Roberts Massif, Schroeder Hill, Mt. Augustana, Bennett Platform, Mt. Heekin, Thanksgiving Valley, and Mt. Franke. Continuous samples were collected every 5 cm until refusal (up to 30 cm) and stored frozen in Whirl-Pak™ bags. All surface (21) and depth profile (25) samples were shipped frozen to The Ohio State University and kept frozen until analyzed.

4.2. Analytical methods

4.2.1. Meteoric ^{10}Be analysis

A total of 30 sub-samples of surface soils from all locations and depth profiles from Roberts Massif, Bennett Platform, and Thanksgiving Valley were sieved to determine the grain size at each location. The percentages of gravel (>2 mm), sand (63 µm-2 mm), and silt (<63 µm) are reported in Table S1. Since there is a strong grain size dependence of meteoric ^{10}Be (little ^{10}Be is carried on coarse (>2 mm) grains (Pavich et al., 1986)) the gravel portion of the sample was not included in the meteoric ^{10}Be analysis. The remaining soil (<2 mm) was ground to fine powder using a shatterbox.

Meteoric ^{10}Be (Table 2) was extracted and purified at the NSF/UVM Community Cosmogenic Facility following procedures originally adapted and modified from Stone (1998). First, 0.5 g of powdered soil was weighed into platinum crucibles and 0.4 g of SPEX ^{9}Be carrier (with a concentration of 1,000 µg mL^{-1}) was added to each sample. The samples were fluxed with a mixture of potassium hydrogen fluoride and sodium sulfate. Perchloric acid was then added to remove potassium by precipitation and later evaporated. Samples were dissolved in nitric acid and precipitated as beryllium hydroxide ($Be(OH)_2$) gel, then packed into stainless steel cathodes for accelerator mass spectroscopy isotopic analysis at the Purdue Rare Isotope Measurement (PRIME) Laboratory. Isotopic ratios were normalized to primary standard 07KNSTD with an assumed ratio of 2.85×10^{-12} (Nishiizumi et al., 2007). We corrected sample ratios with a ^{10}Be/^{9}Be blank ratio of $8.2 \pm 1.9 \times 10^{-15}$, which is the average and standard deviation of two blanks processed alongside the samples. We subtracted the blank ratio from the sample ratios and propagated uncertainties in quadrature.

4.2.2. Nitrate analysis

Separate, un-sieved sub-samples of soil from all locations and depth profiles were leached at a 1:5 soil to water ratio for 24 hours, then filtered through a 0.4 µm Nucleopore membrane filter. The leachate was analyzed on a Skalar San++ Automated Wet Chemistry Analyzer with an SA 1050 Random Access Auto-sampler (Lyons et al., 2016; Welch et al., 2010). Concentrations are reported as NO_3^- (Table S2) with accuracy, as determined using USGS 2015 standard, and precision better than 5% (Lyons et al., 2016).

4.3. Exposure age model

We developed a mass balance using the fluxes of meteoric ^{10}Be to and from Shackleton Glacier region soils to calculate the amount of time which has passed since the soil was exposed (Pavich et al., 1984, 1986). The model assumes that soils that were overlain by glacial ice in the past and are now exposed, accumulated less ^{10}Be than soils that were exposed throughout the glacial periods (Fig. 3). The concentration of meteoric ^{10}Be at the surface (N, atoms g^{-1}) per unit of time (dt) is expressed as a function, where the addition of ^{10}Be is represented as the atmospheric flux to the surface (Q, atoms cm^{-2} yr^{-1}), removal due to radioactive decay is represented by a disintegration constant (λ, yr^{-1}), and erosion (E, cm yr^{-1}) is with respect to soil density (ρ, g cm^{-3}) (Eq. 1). Particle mobility into the soil column is represented by a diffusion constant (D, cm^2 yr^{-1}) multiplied by a concentration gradient.

$$\frac{dN}{dt} = Q - \lambda N - E\frac{dN}{dz} - D\frac{d^2N}{dz^2} \quad (1)$$

However, this function is highly dependent on dz, which represents an unknown value of depth into the soil column which is influenced by meteoric ^{10}Be deposition and removal. Additionally, the soil diffusion term is unconstrained and likely varies with depth. We accounted for these uncertainties and other uncertainties regarding ^{10}Be migration in the soil column by calculating the inventory (I, atoms cm^{-2}) of the soil (Eq. 2), assuming that Q had not changed systematically over the accumulation interval (Graly et al., 2010; Pavich et al., 1986). The inventory is the total sum of meteoric ^{10}Be atoms in the soil profile and the change in inventory due to deposition, decay, and surface erosion is related surface exposure age (Eq. 3).

$$I = \sum N \cdot \rho \cdot dz \quad (2)$$

$$\frac{dI}{dt} = Q - \lambda I - EN \quad (3)$$

If the inventory of meteoric ^{10}Be in the soil profile, the concentration at the surface, and soil density are known, and published values for erosion and ^{10}Be flux to the surface are used, we can combine Eqs. (1-3), and solve for time (t, years) (Eq. 4).

$$t = -\frac{1}{\lambda} \cdot \ln\left[1 - \frac{\lambda I}{Q - E\rho N}\right] \quad (4)$$

Equation (4) provides a maximum exposure age assuming that the soil profile did not contain meteoric ^{10}Be before it was exposed to the surface ($N_0 = 0$). Since our exposure age dating technique relies on the number of ^{10}Be atoms within the sediment column (I), any pre-existing ^{10}Be atoms in the soil ($N_0 \neq 0$) causes the calculated age to be an overestimate (Fig. 3c-d) (Graly et al., 2010). Meteoric ^{10}Be concentrations typically decrease with depth until they reach a "background" level (Graly et al., 2010). The background is identified as the point where the concentration of meteoric ^{10}Be is constant with depth ($\frac{dN}{dz} = 0$). Typically, the background values can be used to calculate an initial inventory (I_i, atoms cm^{-2}) using Eq. (5), where N_z is the ^{10}Be concentration (atoms g^{-1}) at the bottom of the profile (z, cm), and correct the observed total inventory (Eq. 6). In this case, we assume that the initial concentration of meteoric ^{10}Be is isotropic. However, an accurate initial inventory can only be determined for soil profiles which decrease in ^{10}Be concentrations to background levels due to the downward transport of ^{10}Be from the surface. This may not be the case in areas of permafrost where ^{10}Be is restricted to the active layer (Bierman et al., 2014).

$$I_i = N_z \cdot \rho \cdot z \quad (5)$$

$$t = -\frac{1}{\lambda} \cdot \ln\left[1 - \frac{(I - I_i)\lambda}{Q - E\rho N}\right] \quad (6)$$

Additionally, the initial inventory can be influenced by repeated glacial advance and retreat during glacial-interglacial cycles. For this case, the soil has "inherited" ^{10}Be during each subsequent exposure to the atmosphere, some of which may have been removed with eroded soil (Fig. 3c-d). For constructional landforms, such as moraines, the inheritance is equal to the background/initial inventory. Without information on drift sequences, it is difficult to correct the measured inventory for inheritance by distinguishing meteoric ^{10}Be that was deposited after the most recent ice retreat from ^{10}Be that was deposited during previous interglacial periods. Instead, only ages that represent total time of exposure through glacial-interglacial cycles, likely as overestimates, can be reported with confidence.

4.3.1. Model variable selection and key assumptions

The exposure age calculations are dependent on the selected values for the variables in Eq. (1-6). We chose a flux value (Q) of 1.3 x 10^5 atoms cm^{-2} yr^{-1} from Taylor Dome (Steig et al., 1995) due to a similar climate to that of the CTAM and an absence of local meteoric ^{10}Be flux data. Soil density (ρ) across the Shackleton Glacier region was approximately 2 g cm^{-3}. While we did not calculate erosion rates, previous studies have estimated rates from rocks of 1 to 65 cm Ma^{-1} in Victoria Land (Ivy-Ochs et al., 1995; Margerison et al., 2005; Morgan et al., 2010; Strasky et al., 2009; Summerfield et al., 1999) and 5 to 35 cm Ma^{-1} further south in the Transantarctic Mountains (Ackert and Kurz, 2004; Balter-Kennedy et al., 2020; Morgan et al., 2010). Balter-Kennedy et al. (2020) determined that erosion rates for boulders at Roberts Massif which were less than 2 cm Ma^{-1}. However, we chose a conservative value of 5 cm Ma^{-1} for our analysis of the Shackleton Glacier region.

It is important to note two key assumptions in our variable selection and model development. First, we have assumed a uniform erosion rate across the region. Given the variety of surface features at each location (Table 2), some locations on valley floors, for example, may have increased surface concentrations of meteoric ^{10}Be due to entrapment of wind-blown fine-grained sediments. Locations on hillslopes and valley walls might have higher erosion rates (Morgan et al., 2010; Schiller et al., 2009). We assumed that deflation of fine-grained material had occurred rapidly on the flat surfaces we sampled due to strong winds over the poorly consolidated tills following soil exposure (Lancaster et al., 2010). Due to a deficit of soil erosion data in the CTAM, we calculated exposure ages (Eq. 6) with the 5 cm Ma^{-1} erosion value and without the erosion/deposition term (E=0). Second, we attempted to estimate the background concentrations and initial inventory for each sample collected furthest from the glacier. We hypothesized that these samples were potentially exposed throughout at least the LGM and had negligible inheritance, though this was merely an assumption. With the possibility of overestimating or underestimating the exposure ages, we solved Eq. 6 both with and without estimated initial inventory terms. For all samples, including those without depth profile measurements, we utilized an empirical relationship derived between surface/maximum meteoric ^{10}Be concentration and measured inventory to estimate surface exposure ages (see Section 5.3.3) (Graly et al., 2010). Regarding our NO_3^- measurements, we assumed that aside from solubilization and salt translocation, NO_3^- is preserved in the soils and any volatilization or photolysis is negligible (Diaz et al., 2020; Jackson et al., 2016).

5. Results

5.1. Concentrations of meteoric ^{10}Be and depth profile composition

Sediment grain size is similar among the three soil profiles collected from Roberts Massif, Bennett Platform, and Thanksgiving Valley; the soils are primarily comprised of sand-sized particles, with less silt-sized and smaller material (Fig. 4). The proportions of silt and gravel are similar at Roberts Massif, although the majority of the profile is sand-sized. Thanksgiving Valley has the least fine material, while Bennett Platform has a more even grain size distribution. The deepest profile is from Thanksgiving Valley, while the Roberts Massif and Bennett Platform profiles are half the depth. All three profiles are ice-cemented at the bottom and are shallow compared those collected from the McMurdo Dry Valleys (Dickinson et al., 2012b; Schiller et al., 2009; Valletta et al., 2015).

Surface concentrations of meteoric ^{10}Be span more than an order of magnitude in the Shackleton Glacier region and range from 2.9 x 10^8 atoms g^{-1} at Mount Speed to 73 x 10^8 atoms g^{-1} at Roberts Massif (Fig. 5; Table 3). At individual sites where samples were collected at two locations, concentrations are typically highest for the samples furthest from the glacier, with notable exceptions at Roberts Massif and Thanksgiving Valley (Fig. 5). This trend is expected since our sampling plan was designed to capture both recently exposed soils (near the glacier(s)) and soils which have been exposed throughout the LGM and possibly other glacial periods. The measured inventories (Eq. 2) vary from 0.57 x 10^{11} atoms at Bennett Platform to 1.5 x 10^{11} atoms at Roberts Massif (Table 4).

The meteoric ^{10}Be depth profiles differ between Roberts Massif, Thanksgiving Valley, and Bennett Platform. The profile from Roberts Massif has the highest overall concentrations (Fig. 6). Within the profile, the 5-10 cm sampling interval has the highest concentration, followed by the bottom of the profile, then the surface. The profile behavior for Thanksgiving Valley is similar, though the differences in concentrations within both profiles are relatively small. Bennett Platform is the only location where the surface concentration is the highest compared to the remainder of the profile, which decreases with depth (Fig. 6). Although we sampled the entirety of the active layer where particle mobility throughout the soil column occurs, no depth profiles appear to decrease to background levels needed to calculate an initial meteoric ^{10}Be inventory (Eq. 5). As a result, we are not able to correct the measured inventory for background ^{10}Be nor are we able estimate the inherited ^{10}Be concentration in the soil (Eq. 6).

5.2. Relationship between meteoric ^{10}Be and NO_3^-

Measured concentrations of NO_3^- span four orders of magnitude across the seven depth profiles sampled in the Shackleton Glacier region (Fig. S1; Table S2). The lowest concentration is from Mt. Franke, ~1 μg g^{-1}; the highest concentration is from Roberts Massif, 15 mg g^{-1}. In addition, similar to the meteoric ^{10}Be profiles, the NO_3^- concentrations are highest for the samples that were collected furthest from the coast and at the highest elevations (Table S2). The concentrations of NO_3^- and meteoric ^{10}Be are compared for Roberts Massif, Bennett Platform, and Thanksgiving Valley (Fig. 6b). In general, the profiles from Roberts Massif and Thanksgiving Valley are similar, where ^{10}Be and NO_3^- concentrations are highest just below the surface in the 5-10 cm interval and are fairly consistent throughout the profile. The NO_3^- depth profile mirrors the ^{10}Be profile at Bennett Platform – while ^{10}Be concentrations decrease with depth, the NO_3^- concentration increases with depth.

Since the behaviors of NO_3^- and ^{10}Be are parallel or mirrored (as in the case for Bennett Platform), we further evaluate their relationship. When regressed on log scales, NO_3^- and ^{10}Be have a strong power-law relationship with R^2 values ranging from 0.66 to 0.99 (Fig. 6c). The power-law slope for Roberts Massif and Thanksgiving Valley is positive, while the Bennett Platform has a negative slope. Given this regressed relationship, it is possible to estimate ^{10}Be concentrations using NO_3^- concentrations (see Section 5.3.2).

5.3. Relative exposure age calculations and estimates

5.3.1 "Measured" exposure ages from Roberts Massif, Bennett Platform, and Thanksgiving Valley

We calculated exposure ages for the samples furthest from the glacier for Roberts Massif, Bennett Platform, and Thanksgiving Valley using Eq. 4, both with and without the erosion term (Table 3). The exposure ages with erosion range from 120 ka to 4.15 Ma, and the ages without erosion range from 110 ka to 1.67 Ma for Bennett Platform and Roberts Massif, respectively. Thanksgiving Valley is intermediate with an exposure age of 540 ka with erosion and 500 ka without erosion. Since we are not able to correct for initial inventory or inheritance, the exposure ages with the erosion term represent maximum ages. The erosion rate we estimated is relatively low compared to the calculated exposure ages for most samples and would only slightly influence the measured exposure ages. Roberts Massif is an exception where the inclusion

or exclusion of erosion alters the measured age by over 50%. Moreover, the ages without erosion terms are probably overestimates as well without inheritance corrections.

5.3.2 "Estimated" exposure ages using NO_3^- relationship

As we suggest in Section 5.2, the power-law relationship between NO_3^- and meteoric ^{10}Be can be used to estimate ^{10}Be concentrations from NO_3^- concentrations. Since we measured NO_3^- concentrations in all seven depth profiles, we compared the profile concentrations and shape from the four profiles without ^{10}Be depth measurements (Mt. Augustana, Schroeder Hill, Mt. Franke, and Mt. Heekin) to the Roberts Massif, Bennett Platform, and Thanksgiving Valley profiles with both measurements (Fig. S1). Our calculation fundamentally assumes no loss of NO_3^- due to prolonged surface exposure and that NO_3^- profiles which have similar shapes among the sites might have similar ^{10}Be profile shapes as well. The profiles are all fairly homogenous and most similar to the profile from Thanksgiving Valley, though Schroeder Hill is most similar to Roberts Massif (Fig. S1). Applying the power-law relationship from Thanksgiving Valley to Mt. Augustana, Mt. Franke and Mt. Heekin, and the relationship from Roberts Massif to Schroeder Hill, we provide estimates of meteoric ^{10}Be concentrations for the entire depth profile (Table S2) and use these concentrations to calculate an "estimated" inventory using Eq. 2 (Table 4). Further, the estimated inventories are used to estimate exposure ages using Eq. 4, both with and without the erosion term.

The estimated inventories (using the NO_3^- power-law relationship) with erosion range from 0.14×10^{11} atoms at Bennett Platform to 1.5×10^{11} atoms at Roberts Massif (Table 4). The measured and estimated inventories differ by ~3-18%. The estimated exposure ages using the estimated inventory range from 120 ka to 4.54 Ma with erosion, and the ages without erosion range from 110 ka to 1.74 Ma for Bennett Platform and Roberts Massif, respectively (Table 4). The measured and NO_3^- estimated exposure ages, both with and without erosion, only differ by ~4-20% for Roberts Massif, Bennett Platform, and Thanksgiving Valley. Since we cannot calculate exposure ages using only ^{10}Be for the profiles from Schroeder Hill, Mt. Augustana, Mt. Heekin, and Mt. Franke, we are not able to make similar age comparisons. However, we can compare the estimated surface ^{10}Be concentrations using NO_3^- to the measured ^{10}Be concentrations. The percent differences at Schroeder Hill and Mt. Heekin are 4% and 7%, respectively, while Mt. Augustana and Mt. Franke have higher differences of 36% and 40%, respectively (Tables 3 and S2).

5.3.3 "Inferred" exposure ages using inventory relationship

Similar to our exposure age estimates using NO_3^- concentrations, we used the relationship between the maximum meteoric ^{10}Be concentration in the soil profile and the meteoric ^{10}Be inventory (Graly et al., 2010) to "infer" ^{10}Be inventories and calculate maximum exposure ages for all eleven locations, again, with and without erosion (Fig. 7; Table 5). As is the case for Roberts Massif and Thanksgiving Valley, the highest concentrations may not always be at the surface for all locations; however, the relationship is sufficiently strong to provide an estimate of the ^{10}Be inventory and thus an age estimate (Fig. 7). Compared to the measured inventories from Roberts Massif, Bennett Platform, and Thanksgiving Valley, the inferred inventories differ by ~16-130%. The inferred exposure ages with erosion range from 58 ka to >6.5 Ma, and the ages without erosion range from 57 ka to 1.94 Ma for Mt. Speed and Roberts Massif, respectively (Table 4). With the exception of Roberts Massif, Thanksgiving Valley, and Mt. Speed, the oldest surfaces are those which we sampled furthest from the glacier, which is consistent with our sampling methodology to capture younger and older soils. The sample from Roberts Massif collected closest to the glacier has an estimated exposure age that is outside the model limits (>6.5 Ma). The measured exposure ages and the inferred exposure ages differ by ~49-75% with erosion and ~15-75% without erosion. The greatest differences between the ages are at Bennett Platform.

6. Discussion

Meteoric ^{10}Be concentrations and surface exposure ages vary widely across the Shackleton Glacier region and at individual locations. Although these data are only measurements from discrete points on the landscape, they constrain relative terrestrial exposure ages. These meteoric ^{10}Be and NO_3^- data contribute to growing exposure age measurements, which can inform climate, landscape development, and biogeography. The Shackleton Glacier region soil profiles have the highest meteoric ^{10}Be concentrations (~10^9 atoms g^{-1}) yet measured in Earth's polar regions (Fig. 6a). Though our profiles are shallower than profiles from the MDV and Victoria Land in Antarctica (Dickinson et al., 2012a; Schiller et al., 2009; Valletta et al., 2015) and Sweden and Alaska in the Arctic (Bierman et al., 2014; Ebert et al., 2012), the soils from these previous studies reached background concentrations of ^{10}Be within the top 40 cm, which is close to our maximum depth of 30 cm at Thanksgiving Valley. The Bennett Platform soil profile is most similar to the soil profiles from other regions in

Antarctica, as they have decreasing ^{10}Be concentrations with depth, while Thanksgiving Valley and Roberts Massif are relatively homogenous and more similar to profiles from the Arctic.

6.1. Calculated, estimated, and inferred exposure age validation

Considering the novelty of our approach, we sought to test and externally validate the exposure ages. Our calculated, estimated, and inferred exposure ages are consistent with the limited *in-situ* exposure age data from the Shackleton Glacier region (http://antarctica.ice-d.org; Balco, 2020). Exposure ages from glacial erratic boulders using *in-situ* cosmogenic measurements were determined in previous studies (Balter-Kennedy et al., 2020; Balco, 2020; http://antarctica.ice-d.org) from Roberts Massif, Thanksgiving Valley, and Mt. Franke (Figs. 8 and 9). From *in-situ* ^{10}Be, ^{26}Al, ^{3}He, and ^{21}Ne data, exposure ages on the northern flank of Roberts Massif range from 1.10 Ma to 3.26 Ma (Balter-Kennedy et al., 2020; Balco, 2020; http://antarctica.ice-d.org), and our measured, estimated, and inferred ages without erosion are 1.67 Ma, 1.74 Ma, and 1.94 Ma, respectively. Our ages, which are likely overestimates due to a lack of initial inventory or inheritance corrections, are comparable to these nearby *in-situ* ages at similar elevations (Figs. 8 and 9). The ages with the erosion term are greater and outside the range from Balter-Kennedy et al. (2020). This suggests that soil erosion rates are probably low at Roberts Massif, and the initial inventory and ^{10}Be inheritance from previous exposures are likely significantly smaller than the measured inventory. Otherwise, the corrected meteoric ^{10}Be exposure ages would be much greater than the *in-situ* ages.

To the north, the *in-situ* ages from erratic boulders at Thanksgiving Valley vary greatly from ~4.3 ka near the glacier to 450 ka at higher elevations, though most ages appear to be around 30 ka (Figs. 8 and 9) (Balco, 2020; http://antarctica.ice-d.org). Our exposure ages are greater than most previous ages. In particular, the sample collected closest to Shackleton Glacier has an inferred age two orders of magnitude higher than the *in-situ* age from a nearby glacial erratic at the same elevation (Fig. 9). Given the location (~100 m from the glacier) and young nearby *in-situ* age (~4.3 ka), this location was likely covered during the LGM and other glacial periods. Therefore, considering the high surface concentration of meteoric ^{10}Be for this sample, it is possible that there is an additional delivery mechanism of ^{10}Be, such as deposition of material deflated from the valley walls or at high elevations, or an otherwise large inherited component.

Closer to the Ross Ice Shelf, the *in-situ* ages from Mt. Franke range from ~29 ka to 220 ka. Our estimated age without erosion is at the top that range at 220 ka, though the inferred ages are considerable younger at 94 ka and 72 ka (Table 5). Similar to Roberts Massif, our ages from Mt. Franke ages are comparable to the *in-situ* ages from similar elevations (Fig. 9). Here, soil erosion, initial inventory, and inheritance likely minimally influence the measured ^{10}Be inventory. We argue that while the measured, estimated, and inferred ages from the Shackleton Glacier region are similar to *in-situ* ages, they are likely an overestimate and most useful from a relative perspective in understanding which surfaces have been exposed for longer than others.

6.2. NO_3^- as an efficient inventory and exposure age estimation tool

This is the first study to use NO_3^- concentrations to directly estimate meteoric ^{10}Be concentrations study, but not the first to attempt to use water-soluble NO_3^- and salts to help understand glacial history. Previous studies have argued that atmosphere-derived salt concentrations at the surface may correlate with exposure ages and wetting ages in Antarctica (Graham et al., 2002; Graly et al., 2018; Lyons et al., 2016; Schiller et al., 2009). Graly et al. (2018) showed that, in particular, water-soluble NO_3^- and boron exhibited the strongest relationships with exposure age (R^2 = 0.9 and 0.99, respectively). Lyons et al. (2016) used nitrate concentrations to estimate the amount of time since the soils were last wetted and Graham et al. (2002) attempted to calculate exposure ages using the inventory of nitrate in the soil. Graly et al. (2018) argue that boron is preferable to nitrate due to concerns related to nitrate mobility under sub-arid conditions (e.g. Frey et al., 2009; Michalski et al., 2005), and given that uncertainties in local accumulation rates and ion transport can result in inaccurate ages when using NO_3^- alone (Graham et al., 2002; Schiller et al., 2009). Based on the results presented here for hyper-arid CTAM ice-free regions and the concerns with boron mobility depending on whether the B species present in the soils is BO_3^{3-} (borate) or H_3BO_3 (boric acid), we conclude that NO_3^- appears suitable for relative age dating and for producing age estimates.

We show that the differences between measured ^{10}Be inventories and estimated inventories using NO_3^- are low (see Section 5.3.2) and argue that the power-law relationship between meteoric ^{10}Be and NO_3^- can be used to expand our current exposure age database for the TAM; compared to cosmogenic radionuclide analyses, NO_3^- analyses are rapid and cost effective. However, a model using NO_3^- or salts alone is likely insufficient, unless the anion accumulation rates are known

(Graham et al., 2002; Schiller et al., 2009). Though the regressions between NO_3^- and ^{10}Be are strong (Fig. 6c), each of the three profiles from Roberts Massif, Bennett Platform, and Thanksgiving Valley have different regression coefficients and slopes. In other words, the nature of the relationship between meteoric ^{10}Be and NO_3^- varies across the Shackleton Glacier region and varies depending on the location. This is likely due to differences in NO_3^- and ^{10}Be transport and mobility in different surface environments and under different local climates. To address these uncertainties, some ^{10}Be data (surface samples for all locations and a few depth profiles) are necessary to constrain the most accurate regression and minimize the associated error.

We tested our meteoric ^{10}Be – NO_3^- model with data from Arena Valley in the MDV (Graham et al., 2002) and found that our model is applicable to other TAM ice-free areas. Similar to the Shackleton Glacier region soils, the soils from Arena Valley are hyper-arid with high concentrations of NO_3^- and other salts (Graham et al., 2002). Precipitation in the MDV is low at ~5 cm water equivalent each year (Fountain et al., 1999), though NO_3^- and other water-soluble salts at the surface can be wetted and mobilized. The highest NO_3^- concentrations are at 10 cm depth, while ^{10}Be concentrations are highest at the surface and decrease with depth, indicating vertical transport of NO_3^- through time (Graham et al., 2002). The power-law relationship between ^{10}Be and NO_3^- throughout the profile is weaker for the Arena Valley samples compared to Shackleton Glacier samples; there is a stronger power-law correlation in the top 20 cm ($R^2 = 0.61$) compared to the bottom 70 cm ($R^2 < 0.01$), though the profile is considerably deeper (110 cm). Using the power-law relationship from Bennett Platform, which mostly closely resembles the profile behavior for Arena Valley given the negative regression slope, the estimated inventory is 5.4×10^{10} atoms. The measured inventory is of the same order of magnitude, 1.3×10^{10} atoms, indicating a moderate model fit. Applying the power-law relationship from Arena Valley, the estimated inventory is 9.2×10^9 atoms, which is ~27% lower than the measured inventory. These results indicate that, although the Shackleton Glacier region is nearly 900 km from Arena Valley, the correlation between NO_3^- and meteoric ^{10}Be is widely applicable in hyper-arid soils. However, as stated previously, NO_3^- and meteoric ^{10}Be data are needed to ascertain the general profile and slope behavior within the region. Additionally, though our NO_3^- estimated ages are validated using *in-situ* data from previous studies, the NO_3^- dating tool will need to be further evaluated with additional measurements and erosion, initial inventory, and inheritance corrections.

6.3. Implications for paleoclimate and ice sheet dynamics

Our work demonstrates that NO_3^- and ^{10}Be are correlated in much of the Shackleton Glacier region and this relationship has important implications for understanding landscape disturbance, either by meltwater or glacier overriding. Exposure age data from across Antarctica show that a polar desert regime began in the mid-Miocene and has persisted into modern time (Lewis et al., 2008; Marchant et al., 1996; Spector and Balco, 2020; Valletta et al., 2015). Additionally, Barrett (2013) provides a detailed review of studies focused on Antarctic glacial history, particularly centered around the "stabilist vs. dynamicist" debate concerning the overall stability of the EAIS. Interpreting 40+ years of data from published literature, they conclude that the EAIS is stabile in the interior with retreat occurring along the margins, including at outlet glaciers (Golledge et al., 2012). Given these findings, we would expect NO_3^- and meteoric ^{10}Be concentrations to be correlated in hyper-arid Antarctic soils, such as those from the Shackleton Glacier region, as both constituents are derived from atmospheric deposition with minimal alteration at the surface. The major differences between the two concern transport mechanisms. Meteoric ^{10}Be transport is limited by clay particle mobility and NO_3^- is mobile upon soil wetting. Deviations in the expected relationship between ^{10}Be and NO_3^- can inform knowledge of surface processes in the TAM.

If we assume an "ideal" situation where an undisturbed hyper-arid soil has accumulated meteoric ^{10}Be (Fig. 3a-b), ^{10}Be concentrations would be highest at the surface and decrease to background levels at depth. None of the profiles we sampled and measured for meteoric ^{10}Be and NO_3^- reached background concentrations. All profiles were sampled until frozen soil was reached (or bedrock at Schroeder Hill) (Fig. S1), demonstrating an active layer much shallower than those from the MDV (Graham et al., 2002; Schiller et al., 2009; Valletta et al., 2015). This suggests that ^{10}Be-laden particles were able to migrate deeper in the past and mobility has been relatively recently (within the ^{10}Be half-life) limited to the top ~20 cm for most the Shackleton Glacier region. Though clay particle translocation by percolating water can explain the correlated behavior of ^{10}Be and NO_3^- at Roberts Massif and Thanksgiving Valley, it is unlikely that the region had sufficient precipitation for significant percolation over the last 14 Ma (Menzies et al., 2006). The concentrations of fine particles in the soil profiles also do not change significantly with depth, as would be expected if large precipitation or melt events were frequent (Fig. 4).

Similar to Arena Valley and Wright Valley in the MDV (Graham et al., 2002; Schiller et al., 2009), NO_3^- concentrations are highest just beneath the surface at Roberts Massif, indicating shallow salt migration under an arid climate. These data suggest that the samples furthest inland at Roberts Massif and Thanksgiving Valley have been undisturbed since at least the middle to late Pleistocene given the soil exposure ages. Although meteoric ^{10}Be and NO_3^- at Bennett Platform are mirrored with a negative power-law slope, we argue that the difference is not due to NO_3^- mobility, but instead ^{10}Be deposition. Bennett Platform was the only location we sampled on a large moraine (Fig. 2c), and as such, we would expect minimal inheritance with ^{10}Be decreasing at depth. This is generally the observed behavior, with significantly higher surface concentrations. The NO_3^- profile behavior is similar to those throughout the Shackleton Glacier region, though the concentrations continue to increase with depth, possibly indicating minor percolation of NO_3^- rich brine. What may be considered the "anomalous" data point is the surface concentration of meteoric ^{10}Be. Even though we sampled a constructional landform, the sample was collected between two boulder lines in a small, local depression (~1 m) (Table 2). It is probably no coincidence that this location also has the greatest proportion of fine-grained material in the soil profile. The two boulder lines impede wind flow and act as a sediment and snow trap, resulting in a higher concentration of meteoric ^{10}Be than expected simply from atmospheric deposition. In this case, an additional deposition term (superseding any erosion) needs to be considered to accurately date the moraine, and the current exposure age we measured may be an overestimate.

The youngest surfaces we sampled are those from the lowest elevations and closest to the Ross Ice Shelf (Fig. 10). This is generally consistent with previous glacial modeling studies which show that the greatest fluctuations in glacier height during the LGM were along outlet glacier and ice shelf margins (Golledge et al., 2012; MacKintosh et al., 2011; Mackintosh et al., 2014). However, erosion rates are low throughout Antarctica (Balter-Kennedy et al., 2020; Ivy-Ochs et al., 1995; Morgan et al., 2010) and would not drastically impact our relatively young inferred ages (Fig. 10). Additionally, background concentrations of meteoric ^{10}Be in other Antarctic soil profiles are often approximately one to two order of magnitude lower than surface concentrations (Fig. 6). With these considerations, the Mt. Speed, Mt. Wasko, and Mt. Franke samples were all likely covered by the Shackleton Glacier during the LGM, as well as the lower elevation, closest to the glacier samples from Mt. Heekin, Bennett Platform, and Mt. Augustana. The samples we collected near the head of Shackleton Glacier encompass

a range of ages, where lower elevation soils are relatively younger, though the soils from Schroeder Hill and Roberts Massif have likely been exposed since the early Pleistocene (Fig. 10).

Sirius Group deposits were observed at Roberts Massif and were deposited as the Shackleton Glacier retreated in this region (Fig. 2a). Evidence for a dynamic EAIS is derived primarily from the diamictite rocks (tills) of the Sirius Group, which are found throughout the TAM and include well-documented outcrops in the Shackleton Glacier region, but their age is unknown (Hambrey et al., 2003). Some of the deposits contain pieces of shrubby vegetation, suggesting that the Sirius Group formed under conditions warmer than present with trees occupying inland portions of Antarctica (Webb et al., 1984, 1996; Webb and Harwood, 1991). Sparse marine diatoms found in the sediments were initially interpreted as evidence for formation of the Sirius Group via glacial over riding of the TAM during the warmer Pliocene (Barrett et al., 1992), though it is now argued that the marine diatoms were wind-derived contamination, indicating that the Sirius Group is older (Scherer et al., 2016; Stroeven et al., 1996). We document a large diamictite at site RM2-8 that is underlain by soils with an inferred age of at least 1.9 Ma, possibly greater than 6.5 Ma. These exposure ages suggest that the loose Sirius Group diamict was deposited at Roberts Massif some point after the Pliocene. While these data cannot constrain the age of the formation, we suggest that the diamict could have formed prior to the Pliocene and was transported during the Pleistocene glaciations.

7. Conclusions

We measured concentrations of meteoric ^{10}Be and NO_3^- in soils from eleven ice-free areas along the Shackleton Glacier, Antarctica, which include the highest measured meteoric ^{10}Be concentrations from the polar regions. Measured (using meteoric ^{10}Be inventories), estimated (using the power-law relationship between NO_3^- and ^{10}Be), and inferred (using the relationship between maximum ^{10}Be and total inventory) exposure ages were calculated and ranged from 58 ka to >6.5 Ma with an estimated erosion component and 57 ka to 1.9 Ma without erosion. In general, there is good agreement between the three techniques.

The estimated and inferred ages without erosion at Roberts Massif, Thanksgiving Valley, and Mt. Frank are similar to nearby *in-situ* ages from previous studies. In particular, relating NO_3^- concentrations to ^{10}Be measurements results an efficient method to attain a greater number of exposure ages in the CTAM, a region with currently sparse meteoric ^{10}Be data.

However, the power-law relationship between NO_3^- and ^{10}Be had either a positive or negative slope depending on the location, therefore the widespread applicability of this tool needs to be further evaluated. Additionally, though we assumed an erosion rate for the region, some soils in local topographic lows probably have a positive particle flux.

Since NO_3^- and ^{10}Be are both derived from atmospheric deposition, we expect the shape of their accumulation profiles to be similar at depth in hyper-arid soils. In general, this was true for Roberts Massif and Thanksgiving Valley, while NO_3^- and ^{10}Be concentrations were mirrored at Bennett Platform. We conclude that much of the southern Shackleton Glacier region has maintained persistent arid conditions since at least the Pleistocene, though the region was warmer and wetter in the past, as evidenced by frozen soil at the bottom of our depth profiles. The onset of aridity is particularly important in understanding refugia and ecological succession in TAM soils. Since the region has remained hyper-arid and undisturbed for upwards of a few million years, prolonged exposure has resulted in the accumulation of salts at high concentrations in the soils. As such, it is an enigma how soil organisms have persisted throughout glacial-interglacial cycles. However, it is possible that organisms have survived near the glacier at locations like Mt. Augustana, where glacial advance appears to have been minimal during the LGM, but seasonal summer melt has the potential to solubilize salts.

Overall, our data show that the relatively youngest soils we sampled were at lower elevations near the Shackleton Glacier terminus and lower elevations further inland (typically near the glacier). Our sampling scheme was successful in capturing a range of surface exposure ages which contribute to growing archives in the CTAM. We hope that future studies will address the outstanding issues regarding inheritance dynamics of meteoric ^{10}Be in disturbed environments and particle erosion/deposition rates.

Author Contributions

The project was designed and funded by BJA, DHW, IDH, NF, and WBL. Fieldwork was conducted by BJA, DHW, IDH, NF, and MAD. LBC, PRB, and MAD prepared the samples for meteoric ^{10}Be analysis and MAD analyzed the samples for NO_3^-. MAD wrote the article with contributions and edits from all authors.

Data Availability Statement

The datasets generated for this study are included in the article or supplementary materials.

Competing Interests

The authors declare that they have no conflict of interest.

Acknowledgments

We thank the United States Antarctic Program (USAP), Antarctic Science Contractors (ASC), Petroleum Helicopters Inc. (PHI), and Marci Shaver-Adams for logistical and field support. We especially thank Dr. Marc Caffe and the Purdue University PRIME Lab for their assistance with AMS measurements. Additionally, we thank Dr. Andrew Christ at University of Vermont for thoughtful discussions and Dr. Sue Welch and Daniel Gilbert at The Ohio State University for help with initial laboratory analyses. We appreciate the detailed and thoughtful suggestions and edits from Dr. Brent Goehring and an anonymous reviewer which have greatly improved this manuscript. This work was supported by NSF OPP grants 1341631 (WBL), 1341618 (DHW), 1341629 (NF), 1341736 (BJA), NSF GRFP fellowship 60041697 (MAD), and a PRIME Lab seed proposal (MAD). Sample preparation and LBC's time supported by NSF EAR 1735676. Geospatial support for this work provided by the Polar Geospatial Center under NSF OPP grants 1043681 and 1559691.

Figures:

Figure 1: Overview map of the Shackleton Glacier region, located in the Queen Maud Mountains of the Central Transantarctic Mountains. The red circles represent our eleven sampling locations, with an emphasis on Roberts Massif (orange), Bennett Platform (green), and Thanksgiving Valley (blue), which have the most comprehensive dataset in this study. The bedrock serves as primary weathering product for soil formation (Elliot and Fanning, 2008; Paulsen et al., 2004). Base maps provided by the Polar Geospatial Center.

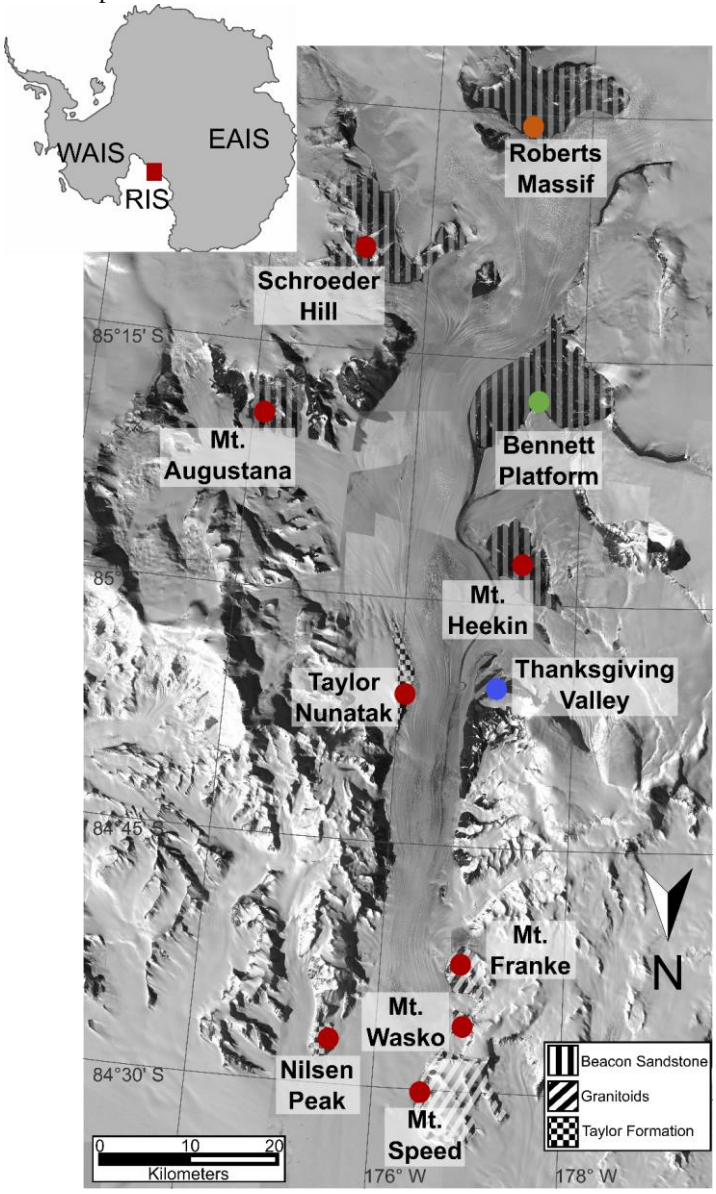

Figure 2: The Sirius Group was documented at Roberts Massif near the RM2-8 sampling location (a). Small moraines were observed at Roberts Massif (b) and large moraines at Bennett Platform (c).

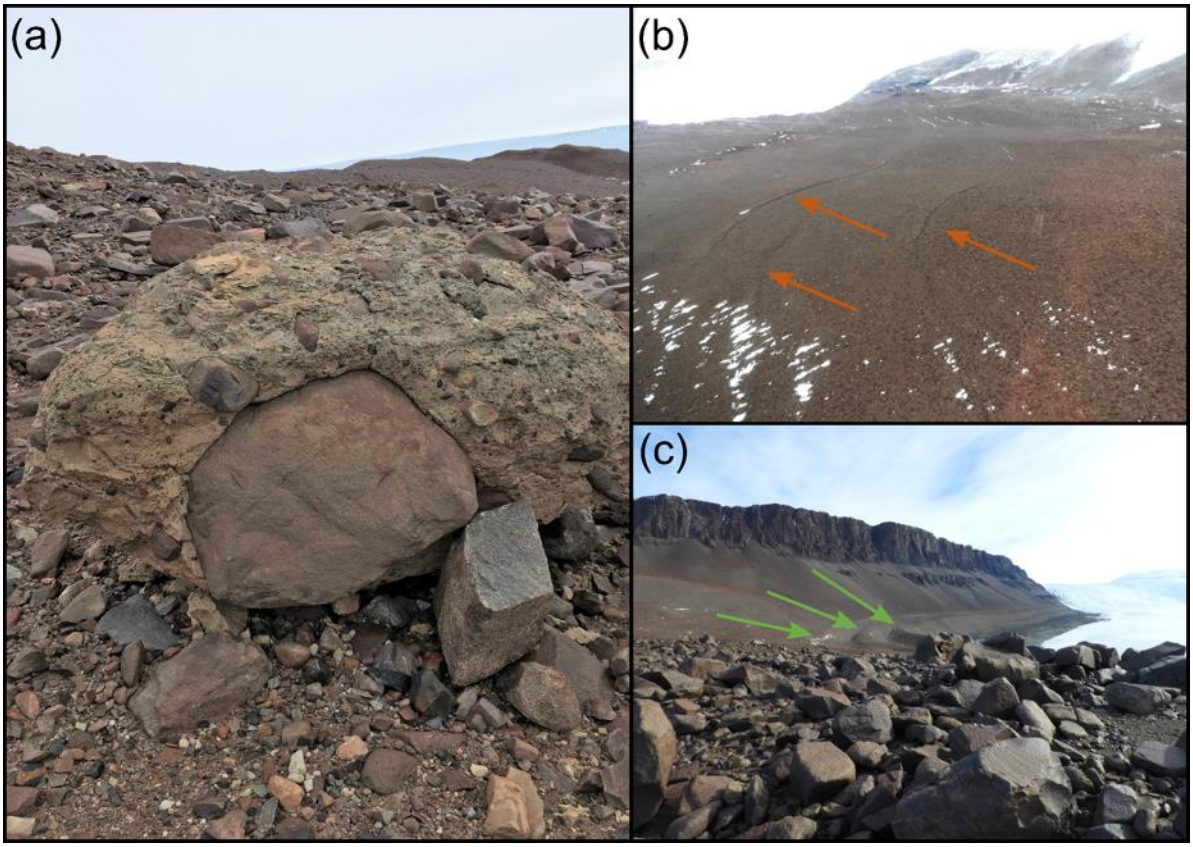

Figure 3: Conceptual diagram of meteoric ^{10}Be accumulation in soils during glacial advance and retreat. In "ideal" conditions, ^{10}Be accumulates in exposed soils and ^{10}Be concentrations beneath the glacier are negligible at background levels (a). As the glacier retreats, ^{10}Be can begin accumulating in the recently exposed soil and an inventory can be measured to calculate exposure ages. In the case where the glacier has waxed and waned numerous times and the soils already contain a non-negligible "inheritance" concentration of ^{10}Be, the inventories need to be corrected for ^{10}Be inheritance (c-d) to accurately determine exposure ages.

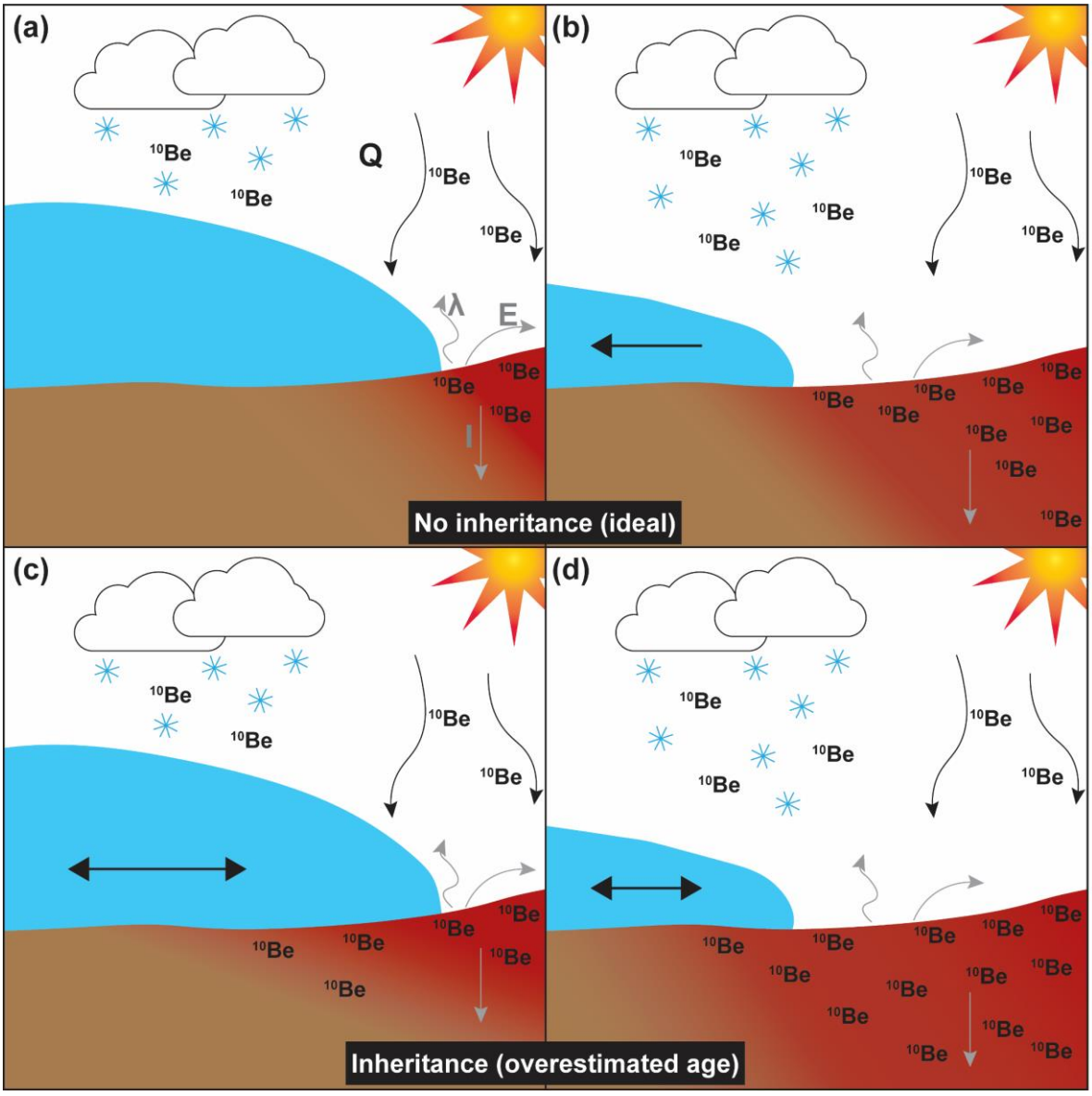

Figure 4: The grain size composition of soil profiles collected from Roberts Massif (a, orange), Bennett Platform (b, green), and Thanksgiving Valley (c, blue). The soil pits from Bennett Platform and Thanksgiving Valley are also shown with distinct soil horizons.

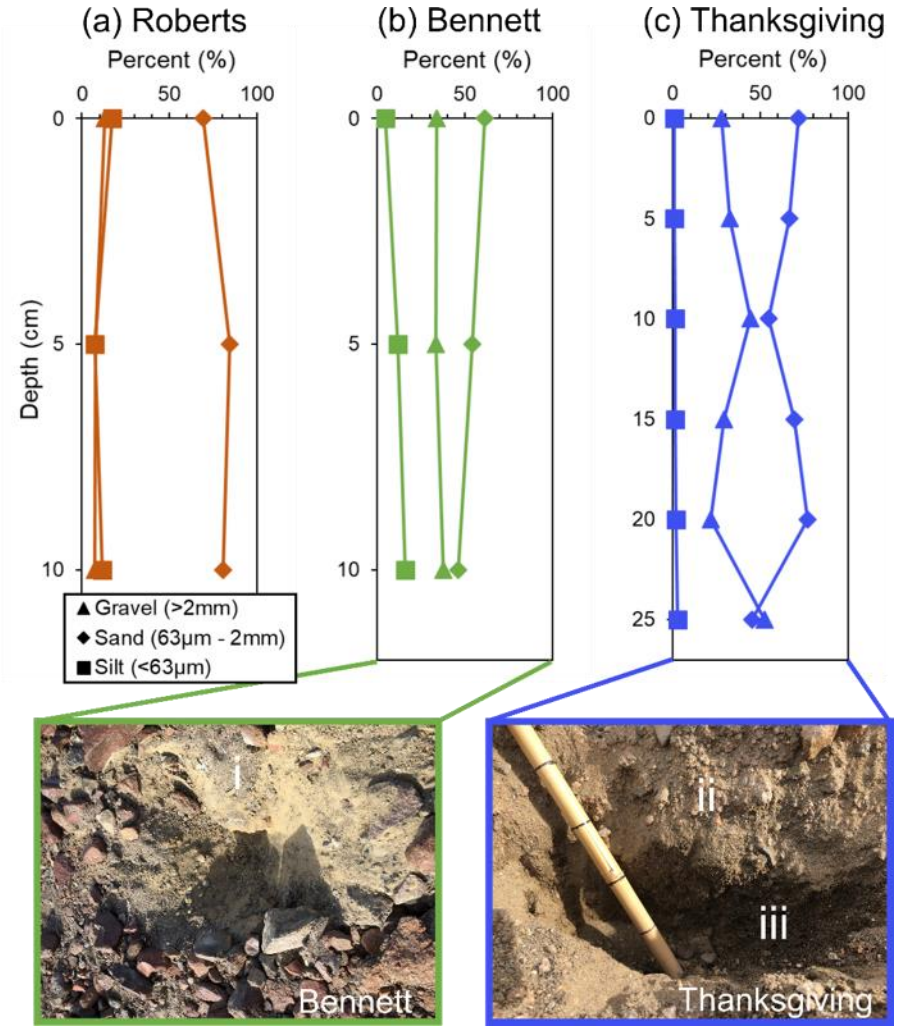

Figure 5: Spatial distribution of surface meteoric ^{10}Be concentrations in the Shackleton Glacier region (a). Where possible, two samples were collected at each location to represent surfaces closest to the glacier, which might have been glaciated during recent glacial periods, and samples furthest from the glacier that are likely to have been exposed during recent glacial periods. Insets of Roberts Massif (b), Bennett Platform (c), and Thanksgiving Valley (d) are included, as these locations serve as the basis for our relative exposure age models. Base maps provided by the Polar Geospatial Center.

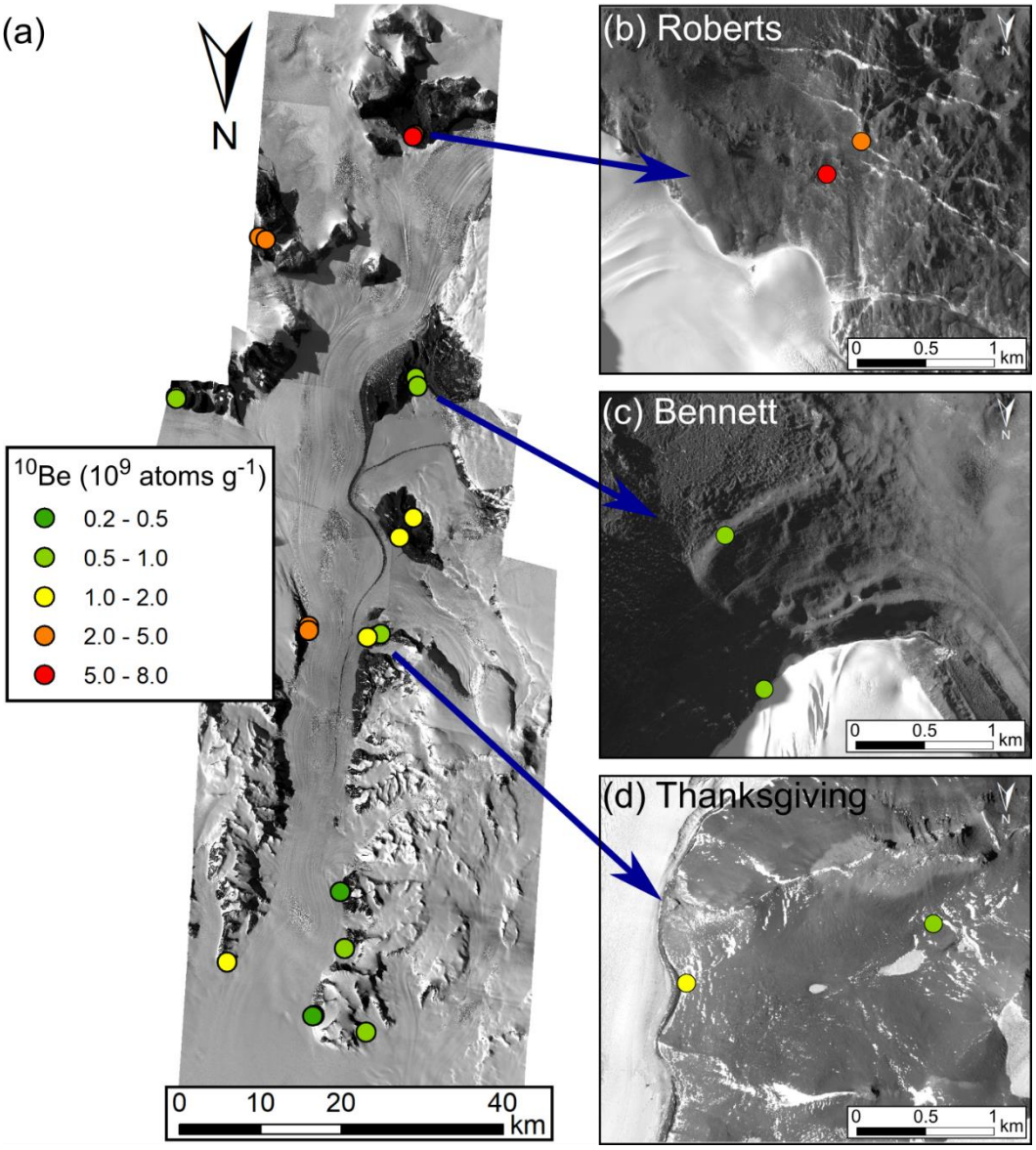

562 **Figure 6:** Soil profiles of meteoric ^{10}Be concentrations for Roberts Massif (orange), Bennett Platform (green), and
563 Thanksgiving Valley (blue) compared to profiles from the Antarctic (Dickinson et al., 2012*; Schiller et al., 2009†; Valletta
564 et al., 2015‡) and Arctic (Bierman et al., 2014¶; Ebert et al., 2012§) (a). The ^{10}Be concentration profiles were also compared
565 to NO_3^- concentration profiles (b) and a power function was fit to the data (c).
566

567

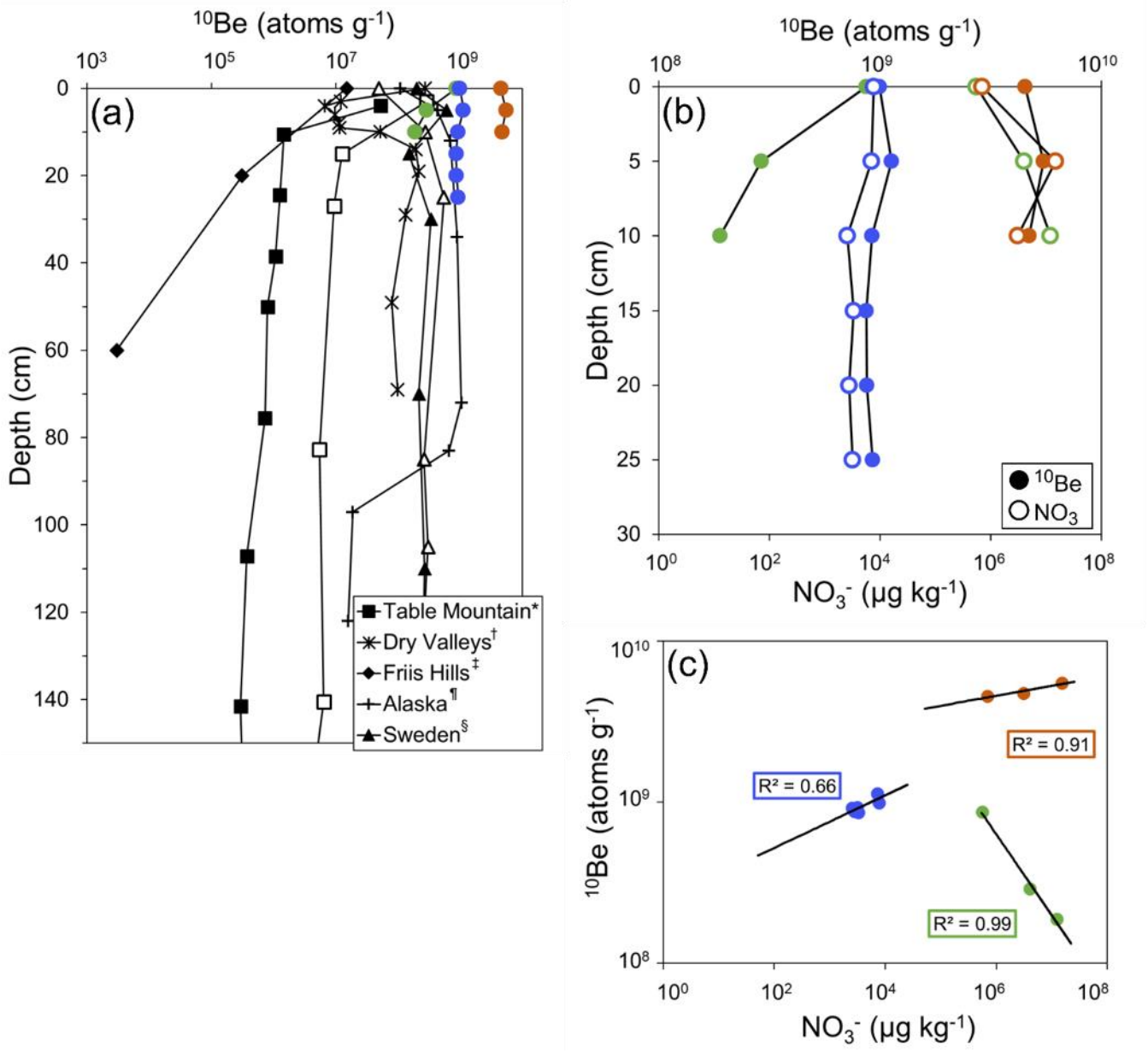

568

569

570 **Figure 7:** Relationship between the measured maximum (or surface) meteoric ^{10}Be concentration and the calculated
571 inventory (Eq. 2). This relationship is used to infer ^{10}Be inventories given a maximum or surface concentration (Graly et al.,
572 2010). The solid black line is the power relationship between concentration and inventory, while the dashed grey line is the
573 regression from Graly et al. (2010).
574

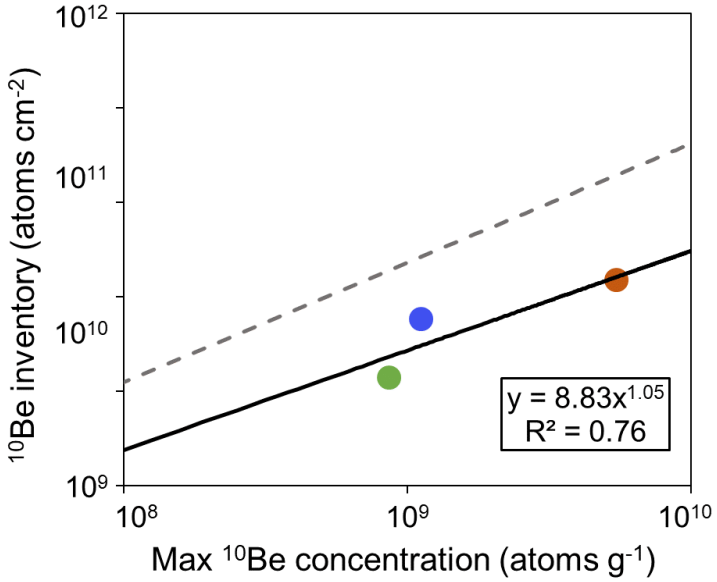

575
576

Figure 8: *In-situ* exposure age measurements from glacial erratic boulders (black filled triangles) (http://antarctica.ice-d.org; Balco, 2020; Balter-Kennedy et al., 2020) in relation to the meteoric ^{10}Be sample locations from Roberts Massif (a, orange), Thanksgiving Valley (b, blue), and Mt. Franke (c, grey). Pleistocene-age moraines described by Balter-Kennedy et al. (2020) are labeled at Roberts Massif in green. We identified moraines (green) of an unknown age at Mt. Franke.

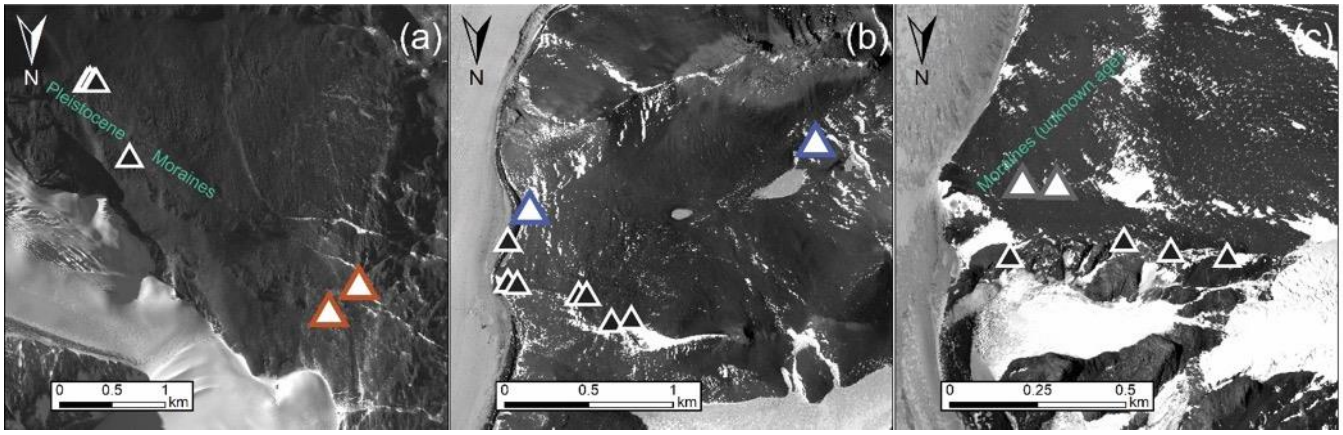

Figure 9: Estimated (using NO_3^-) meteoric ^{10}Be exposure ages (open colored triangles) and inferred (using maximum ^{10}Be concentration) exposure ages (closed colored triangles) without erosion compared to *in-situ* ages from ICE-D (Balco, 2020) and Balter-Kennedy et al. (2020) (solid triangles) against elevation. All *in-situ* ages were measured from glacial erratic boulders.

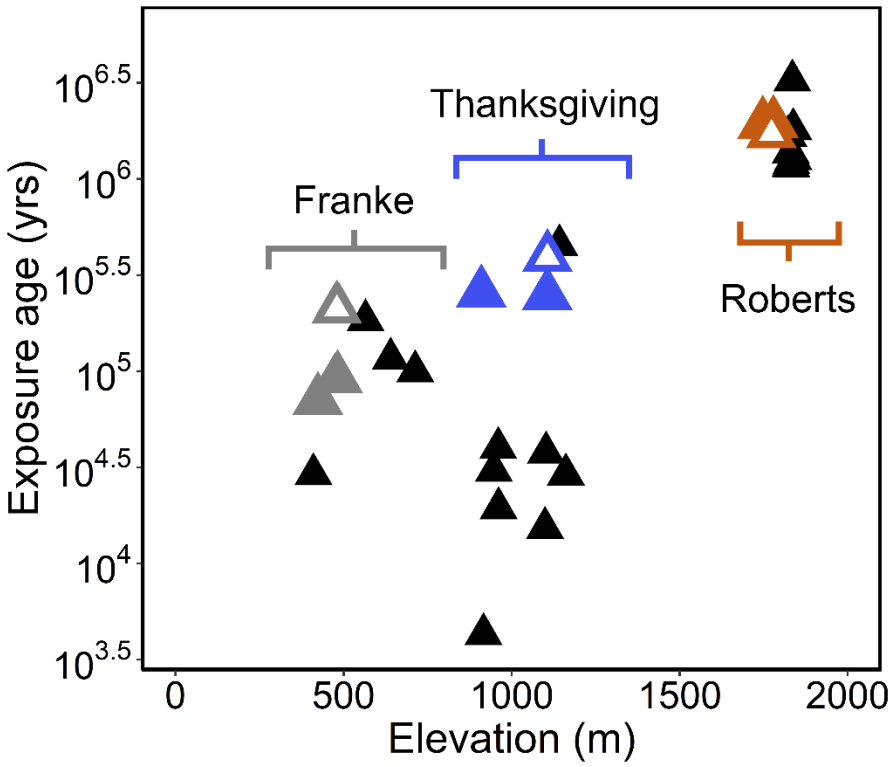

Figure 10: Inferred surface exposure ages versus distance from the coast (a) and elevation (b), with (blue) and without (black) an assumed erosion term. Upward facing triangles are samples collected furthest from the glacier, while downward triangles are samples collected closest to the glacier. The estimated surface exposure ages using NO_3^- concentrations are included in panel (c). Values with asterisks (*) are ages calculated using the measured meteoric ^{10}Be concentrations in depth profiles.

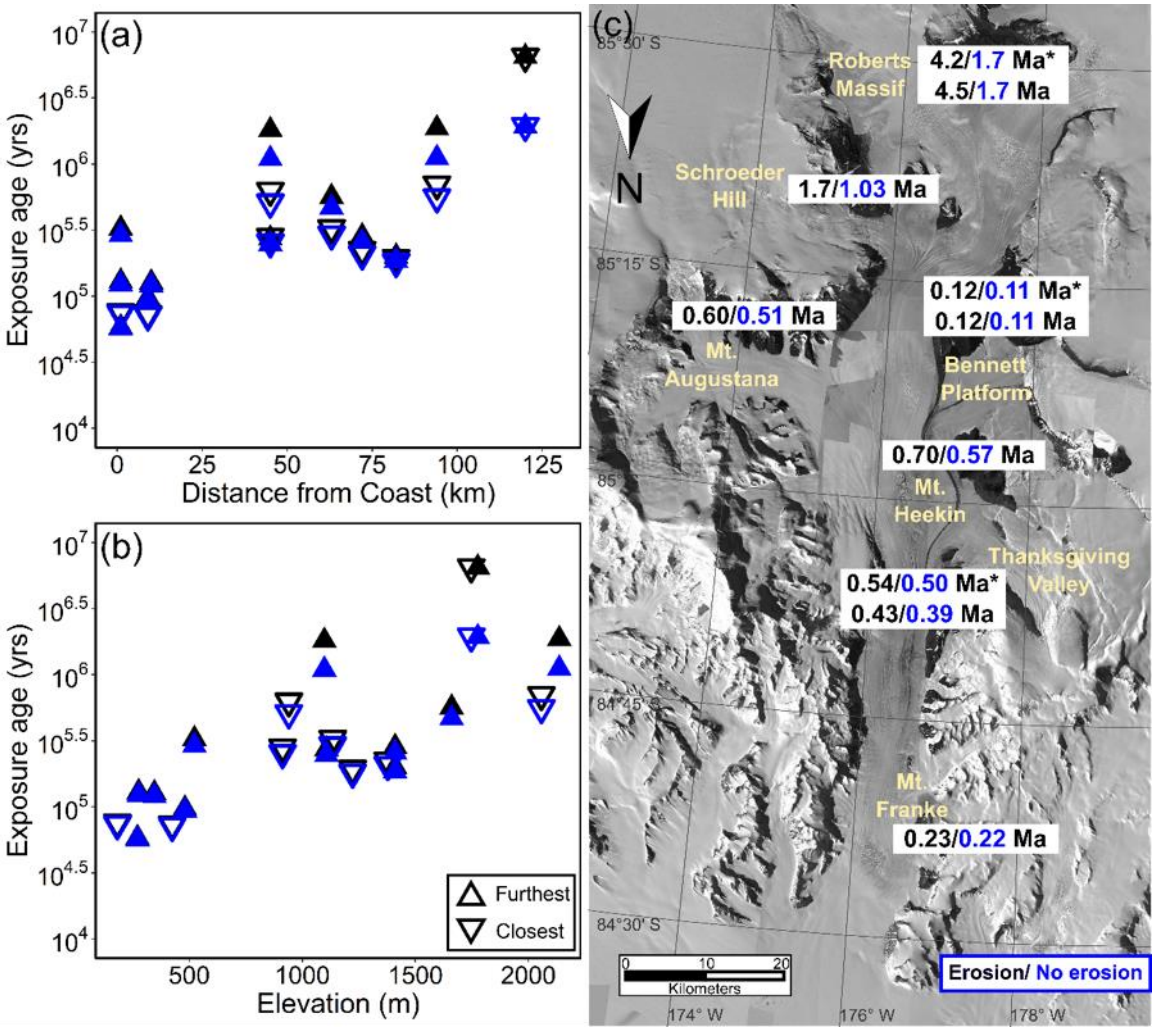

Tables:

Table 1: Geographic data of samples collected from eleven ice-free areas along the Shackleton Glacier. Distance from the coast (aerial) was measured post-collection using ArcMap 10.3 software. Samples of the format "X-1" are samples collected furthest from the glacier in the transect.

Location	Sample name	Latitude	Longitude	Elevation (m)	Distance from coast (km)
Mt. Augustana	AV2-1	-85.1706	-174.1338	1410	72
Mt. Augustana	AV2-8	-85.1676	-174.1393	1378	72
Bennett Platform	BP2-1	-85.2121	-177.3576	1410	82
Bennett Platform	BP2-8	-85.2024	-177.3907	1222	82
Mt. Franke	MF2-1	-84.6236	-176.7353	480	9
Mt. Franke	MF2-4	-84.6237	-176.7252	424	9
Mt. Heekin	MH2-1	-85.0299	-177.2405	1660	63
Mt. Heekin	MH2-8	-85.0528	-177.4099	1134	63
Mt. Speed	MSP2-1	-84.4819	-176.5070	270	0
Mt. Speed	MSP2-4	-84.4811	-176.4864	181	0
Mt. Speed	MSP4-1	-84.4661	-177.1224	276	0
Mt. Wasko	MW4-1	-84.5600	-176.8177	345	10
Nilsen Peak	NP2-5	-84.6227	-176.7501	670	0
Roberts Massif	RM2-1	-85.4879	-177.1844	1776	120
Roberts Massif	RM2-8	-85.4857	-177.1549	1747	120
Schroeder Hill	SH3-2	-85.3597	-175.0693	2137	94
Schroeder Hill	SH3-8	-85.3569	-175.1621	2057	94
Thanksgiving Valley	TGV2-1	-84.9190	-177.0603	1107	45
Thanksgiving Valley	TGV2-8	-84.9145	-176.8860	912	45
Taylor Nunatak	TN3-1	-84.9227	-176.1242	1097	45
Taylor Nunatak	TN3-5	-84.9182	-176.1282	940	45

603 **Table 2:** Surface features of the sample locations from the Shackleton Glacier region.
604

Location	Sample name	Sample description
Mt. Augustana	AV2-1	Up valley from Gallup Glacier (tributary glacier); at valley floor; surface covered by cobbles and pebbles; red-stained sandstones nearby; frozen ground at bottom of depth profile
Mt. Augustana	AV2-8	At toe of Gallup Glacier; surface covered primarily by boulders; mainly sand between boulders
Bennett Platform	BP2-1	On larger moraine; local depression between two boulder lines, up valley from McGregor Glacier (tributary glacier); at valley floor
Bennett Platform	BP2-8	At toe of McGregor Glacier (tributary glacier); surface covered primarily by boulders; mainly sand between boulders
Mt. Franke	MF2-1	Bottom of wide valley floor; near small moraine; frozen soil at bottom of depth profile
Mt. Franke	MF2-4	Bottom of wide valley floor; near small moraine
Mt. Heekin	MH2-1	On high-elevation saddle; surface covered by sparse small boulders, cobbles, and pebbles; poorly consolidated till; frozen ground at bottom of profile
Mt. Heekin	MH2-8	At toe of Baldwin Glacier (alpine glacier) on valley floor; two ponds nearby; surface covered by loose rocks and sand; poorly consolidated till; possible polygonal surface nearby
Mt. Speed	MSP2-1	Steep slope; large granite boulders; scree
Mt. Speed	MSP2-4	Near cliff by Shackleton Glacier; large granite boulders; scree
Mt. Speed	MSP4-1	Spur on level with glacier; frozen soil near 5 cm depth
Mt. Wasko	MW4-1	Steep slope; large granite boulders; scree; nearby snowpack
Nilsen Peak	NP2-5	On ridge; near large snow patch
Roberts Massif	RM2-1	Near thin moraine; red-stained sandstones nearby with etches; frozen ground at bottom of depth profile
Roberts Massif	RM2-8	Near thin moraine and Sirius Group diamict; large boulders nearby with unconsolidated sediment
Schroeder Hill	SH3-2	Red-stained sandstone; poorly consolidated till; bedrock at bottom of profile
Schroeder Hill	SH3-8	Red-stained sandstone; poorly consolidated till;
Thanksgiving Valley	TGV2-1	Lightly uphill on valley wall; poorly consolidated till; frozen ground at bottom of depth profile; polygonal surface nearby
Thanksgiving Valley	TGV2-8	At the toe of Shackleton Glacier; near thin moraines, surface covered primarily large boulders
Taylor Nunatak	TN3-1	On ridge; surface covered by small boulders with underlaying silt; frozen ground at bottom of depth profile
Taylor Nunatak	TN3-5	Valley floor; nearby snow patches; few glacial erratics; surface covered primarily by small boulders and cobbles with underlaying silt

605

606 **Table 3:** Concentration of meteoric ^{10}Be in Shackleton Glacier region surface soils and depth profiles from Roberts Massif, Bennett Platform, and Thanksgiving
607 Valley.
608

Sample name	Sample mass (g)	Mass of ^{9}Be added (µg)*	AMS Cathode Number	Uncorrected $^{10}Be/^{9}Be$ ratio (10^{-11})**	Uncorrected $^{10}Be/^{9}Be$ ratio uncertainty (10^{-13})**	Background-corrected $^{10}Be/^{9}Be$ ratio (10^{-11})***	Background-corrected $^{10}Be/^{9}Be$ ratio uncertainty (10^{-13})***	^{10}Be concentration (10^{9} atoms g^{-1})	^{10}Be concentration uncertainty (10^{7} atoms g^{-1})
AV2-1	0.499	394.3	151135	2.201	1.143	2.201	1.143	1.162	0.604
AV2-8	0.500	400.2	151137	1.786	1.067	1.785	1.067	0.955	0.571
BP2-1, 0-5	0.499	401.2	151147	1.616	1.055	1.615	1.055	0.868	0.567
BP2-1, 5-10	0.499	399.2	151148	0.353	0.748	0.352	0.748	0.188	0.400
BP2-1, 10-15	0.496	400.2	151149	1.573	1.894	1.573	1.894	0.848	1.021
BP2-8	0.498	400.2	151550	0.542	0.448	0.541	0.448	0.291	0.241
MF2-1	0.505	398.2	151554	3.713	3.444	3.712	3.444	1.956	1.815
MF2-4	0.501	398.2	151555	2.448	1.395	2.447	1.396	1.300	0.741
MH2-1	0.498	399.2	151138	0.864	0.820	0.863	0.820	0.462	0.439
MH2-8	0.499	395.3	151139	0.681	0.847	0.680	0.847	0.360	0.449
MSP2-1	0.499	403.2	151556	0.539	0.464	0.538	0.464	0.291	0.250
MSP2-4	0.502	402.2	151557	0.693	0.673	0.692	0.674	0.370	0.361
MSP4-1	0.499	400.2	151566	1.112	1.117	1.111	1.117	0.596	0.598
MW4-1	0.498	400.2	151564	1.093	0.662	1.092	0.662	0.586	0.356
NP2-5	0.496	402.2	151565	2.391	1.200	2.391	1.200	1.295	0.650
RM2-1, 0-5	0.502	399.2	151558	8.541	4.116	8.541	4.116	4.538	2.187
RM2-1, 5-10	0.499	398.2	151559	8.853	8.411	8.852	8.411	4.721	4.485
RM2-1, 10-15	0.500	400.2	151560	13.70	8.460	13.70	8.460	7.327	4.524
RM2-8	0.498	401.2	151561	10.17	15.27	10.17	15.27	5.475	8.221
SH3-2	0.497	398.2	151551	7.191	3.129	7.190	3.129	3.850	1.675
SH3-8	0.501	398.2	151552	4.270	3.351	4.269	3.351	2.267	1.780
TGV2-1, 0-5	0.498	398.2	151140	1.860	2.431	1.859	2.431	0.993	1.299

TGV2-1, 5-10	0.500	398.2	151141	1.731	1.589	1.731	1.589	0.921	0.846
TGV2-1, 10-15	0.497	393.3	151142	1.635	1.377	1.634	1.377	0.864	0.728
TGV2-1, 15-20	0.502	399.2	151143	1.645	1.776	1.645	1.777	0.874	0.944
TGV2-1, 20-25	0.498	403.2	151144	1.711	0.852	1.710	0.852	0.925	0.461
TGV2-1, 25-30	0.497	399.2	151145	2.148	2.071	2.147	2.071	1.152	1.112
TGV2-8	0.499	399.2	151146	2.106	2.185	2.105	2.185	1.125	1.168
TN3-1	0.500	401.2	151562	7.092	5.903	7.091	5.903	3.802	3.165
TN3-5	0.500	401.2	151563	3.926	5.694	3.925	5.694	2.105	3.053
*^{9}Be was added through commercial SPEX carrier with a concentration of 1000 μg mL^{-1}.									
**Isotopic analysis was conducted at PRIME Laboratory; ratios were normalized against standard 07KNSTD3110 with an assumed ratio of 2850 x 10^{-15} (Nishiizumi et al., 2007). Blank ^{10}Be/^{9}Be ratio values averaged 8.152 ± 1.884 x 10^{-15}.									

609

610

611 Table 4: Exposure ages calculated from Eq. (1-6) and estimated ages using NO_3^- concentration data.
612

Location	**Measured inventory (10^{11} atoms)**	**Measured exposure age with *E* (Ma)**	**Measured exposure age without *E* (Ma)**	**Estimated inventory (10^{11} atoms)***	**Estimated exposure age with *E* (Ma)***	**Estimated exposure age without *E* (Ma)***
Augustana	-	-	-	0.580	0.601	0.505
Bennett	0.135	0.115	0.106	0.143	0.122	0.113
Franke	-	-	-	0.268	0.232	0.217
Heekin	-	-	-	0.646	0.703	0.571
Roberts	1.47	4.15	1.67	1.51	4.54	1.74
Schroeder	-	-	-	1.05	1.66	1.03
Thanksgiving	0.570	0.535	0.495	0.465	0.426	0.394
*Estimations derived from linear relationship between NO3- concentration and meteoric 10Be concentration						

613

Table 5: Estimated exposure ages using relationship between maximum ^{10}Be concentration and inventory in Figure S1 (Bierman et al., 2014).

Sample name	Inferred inventory (10^{11} atoms)	Inferred exposure age with *E* (Ma)	Inferred exposure age without *E* (Ma)
AV2-1	0.38	0.285	0.258
AV2-8	0.33	0.224	0.207
BP2-1	0.31	0.200	0.186
BP2-8	0.31	0.195	0.181
MF2-1	0.21	0.097	0.094
MF2-4	0.18	0.074	0.072
MH2-1	0.59	0.565	0.469
MH2-8	0.42	0.328	0.292
MSP2-1	0.16	0.058	0.057
MSP2-4	0.18	0.076	0.074
MSP4-1	0.24	0.129	0.123
MW4-1	0.24	0.127	0.121
NP2-5	0.42	0.326	0.291
RM2-1	1.24	>6.5*	1.93
RM2-8	1.50	>6.5*	1.94
SH3-2	1.07	1.87	1.11
SH3-8	0.67	0.702	0.560
TGV2-1	0.34	0.274	0.248
TGV2-8	0.38	0.282	0.255
TN3-1	1.06	1.81	1.09
TN3-5	0.62	0.628	0.512
*Outside of model range			

References

Ackert, R. P. and Kurz, M. D.: Age and uplift rates of Sirius Group sediments in the Dominion Range, Antarctica, from surface exposure dating and geomorphology, Glob. Planet. Change, 42(1–4), 207–225, doi:10.1016/j.gloplacha.2004.02.001, 2004.

Anderson, J. B., Shipp, S. S., Lowe, A. L., Wellner, J. S. and Mosola, A. B.: The Antarctic Ice Sheet during the Last Glacial Maximum and its subsequent retreat history: a review, Quat. Sci. Rev., 21, 49–70, doi:10.1016/S0277-3791(01)00083-X, 2002.

Augustin, L., Barbante, C., Barnes, P. R. F., Barnola, J. M., Bigler, M., Castellano, E., Cattani, O., Chappellaz, J., Dahl-Jensen, D., Delmonte, B., Dreyfus, G., Durand, G., Falourd, S., Fischer, H., Flückiger, J., Hansson, M. E., Huybrechts, P., Jugie, G., Johnsen, S. J., Jouzel, J., Kaufmann, P., Kipfstuhl, J., Lambert, F., Lipenkov, V. Y., Littot, G. C., Longinelli, A., Lorrain, R., Maggi, V., Masson-Delmotte, V., Miller, H., Mulvaney, R., Oerlemans, J., Oerter, H., Orombelli, G., Parrenin, F., Peel, D. A., Petit, J. R., Raynaud, D., Ritz, C., Ruth, U., Schwander, J., Siegenthaler, U., Souchez, R., Stauffer, B., Steffensen, J. P., Stenni, B., Stocker, T. F., Tabacco, I. E., Udisti, R., van de Wal, R. S. W., van den Broeke, M., Weiss, J., Wilhelms, F., Winther, J. G., Wolff, E. W. and Zucchelli, M.: Eight glacial cycles from an Antarctic ice core, Nature, 429(6992), 623–628, doi:10.1038/nature02599, 2004.

Balco, G.: Technical note: A prototype transparent-middle-layer data management and analysis infrastructure for cosmogenic-nuclide exposure dating, Geochronology, in review(2), 169–175, doi:10.5194/gchron-2020-6, 2020.

Balco, G., Stone, J. O. H., Sliwinski, M. G. and Todd, C.: Features of the glacial history of the Transantarctic Mountains inferred from cosmogenic 26 Al, 10 Be and 21 Ne concentrations in bedrock surfaces, Antarct. Sci., 26(6), 708–723, doi:10.1017/S0954102014000261, 2019.

Balter-Kennedy, A., Bromley, G., Balco, G., Thomas, H. and Jackson, M. S.: A 14.5-million-year record of East Antarctic Ice Sheet fluctuations from the central Transantarctic Mountains, constrained with cosmogenic 3He, 10Be, 21Ne, and 26Al, Cryosph., 14(8), 2647–2672, doi:10.5194/tc-2020-57, 2020.

Barrett, P. J., Adams, C. J., McIntosh, W. C., Swisher, C. C. and Wilson, G. S.: Geochronological evidence supporting Antarctic deglaciation three million years ago, Nature, 359, 816–818, 1992.

Bierman, P. R., Corbett, L. B., Graly, J. A., Neumann, T. A., Lini, A., Crosby, B. T. and Rood, D. H.: Preservation of a Preglacial Landscape Under the Center of the Greenland Ice Sheet, Science (80-.)., 344, 402–405, doi:10.4159/harvard.9780674430501.c21, 2014.

Bromley, G. R. M., Hall, B. L., Stone, J. O., Conway, H. and Todd, C. E.: Late Cenozoic deposits at Reedy Glacier, Transantarctic Mountains: implications for former thickness of the West Antarctic Ice Sheet, Quat. Sci. Rev., 29(3–4), 384–398, doi:10.1016/j.quascirev.2009.07.001, 2010.

Brook, E. J., Kurz, M. D., Ackert, R. P., Denton, G. H., Brown, E. T., Raisbeck, G. M. and Yiou, F.: Chronology of taylor glacier advances in Arena Valley, Antarctica, using in situ cosmogenic 3He and 10Be, Quat. Res., 39(1), 11–23, doi:10.1006/qres.1993.1002, 1993.

Brook, E. J., Brown, E. T., Kurz, M. D., Ackert, R. P., Raisbeck, G. M. and Yiou, F.: Constraints on age, erosion, and uplift of Neogene glacial deposits in the Transantarctic Mountains determined from in situ cosmogenic 10Be and 26Al, Geology, 23(12), 1063–1066, doi:10.1130/0091-7613(1995)023<1063:coaeau>2.3.co;2, 1995.

Brown, E. T., Edmond, J. M., Raisbeck, G. M., Bourlès, D. L., Yiou, F. and Measures, C. I.: Beryllium isotope geochemistry in tropical river basins, Geochim. Cosmochim. Acta, 56(4), 1607–1624, doi:10.1016/0016-7037(92)90228-B, 1992.

Bruno, L. A., Baur, H., Graf, T., Schlüchter, C., Signer, P. and Wieler, R.: Dating of Sirius Group tillites in the Antarctic Dry Valleys with cosmogenic 3He and 21Ne., 1997.

Cary, S. C., McDonald, I. R., Barrett, J. E. and Cowan, D. A.: On the rocks: The microbiology of Antarctic Dry Valley soils, Nat. Rev. Microbiol., 8(2), 129–138, doi:10.1038/nrmicro2281, 2010.

Claridge, G. G. C. and Campbell, I. B.: Origin of nitrate deposits., 1968a.

Claridge, G. G. C. and Campbell, I. B.: Soils of the Shackleton glacier region, Queen Maud Range, Antarctica, New Zeal. J. Sci., 11(2), 171–218, 1968b.

Clark, P. U., Dyke, A. S., Shakun, J. D., Carlson, A. E., Clark, J., Wohlfarth, B., Mitrovica, J. X., Hostetler, S. W. and McCabe, A. M.: The Last Glacial Maximum, Science (80-.)., 325, 710–714, doi:10.1126/science.1172873, 2009.

Collins, G. E., Hogg, I. D., Convey, P., Sancho, L. G., Cowan, D. A., Lyons, W. B., Adams, B. J., Wall, D. H. and Green, T. G. A.: Genetic diversity of soil invertebrates corroborates timing estimates for past collapses of the West Antarctic Ice Sheet, Proc. Natl. Acad. Sci. U. S. A., 117(36), 22293–22302, doi:10.1073/pnas.2007925117, 2020.

Convey, P., Gibson, J. A. E., Hillenbrand, C. D., Hodgson, D. A., Pugh, P. J. A., Smellie, J. L. and Stevens, M. I.: Antarctic terrestrial life - Challenging the history of the frozen continent?, Biol. Rev., 83(2), 103–117, doi:10.1111/j.1469-185X.2008.00034.x, 2008.

Diaz, M. A., Li, J., Michalski, G., Darrah, T. H., Adams, B. J., Wall, D. H., Hogg, I. D., Fierer, N., Welch, S. A., Gardner, C. B. and Lyons, W. B.: Stable isotopes of nitrate, sulfate, and carbonate in soils from the Transantarctic Mountains, Antarctica: A record of atmospheric deposition and chemical weathering, Front. Earth Sci., 8(341), doi:10.3389/feart.2020.00341, 2020.

Dickinson, W. W., Schiller, M., Ditchburn, B. G., Graham, I. J. and Zondervan, A.: Meteoric Be-10 from Sirius Group suggests high elevation McMurdo Dry Valleys permanently frozen since 6 Ma, Earth Planet. Sci. Lett., 355–356, 13–19, doi:10.1016/j.epsl.2012.09.003, 2012a.

Dickinson, W. W., Schiller, M., Ditchburn, B. G., Graham, I. J. and Zondervan, A.: Meteoric Be-10 from Sirius Group suggests high elevation McMurdo Dry Valleys permanently frozen since 6 Ma, Earth Planet. Sci. Lett., 355–356, 13–19, doi:10.1016/j.epsl.2012.09.003, 2012b.

Ebert, K., Willenbring, J., Norton, K. P., Hall, A. and Hättestrand, C.: Meteoric 10 Be concentrations from saprolite and till in northern Sweden: Implications for glacial erosion and age, , doi:10.1016/j.quageo.2012.05.005, 2012.

Elliot, D. H. and Fanning, C. M.: Detrital zircons from upper Permian and lower Triassic Victoria Group sandstones, Shackleton Glacier region, Antarctica: Evidence for multiple sources along the Gondwana plate margin, Gondwana Res., 13, 259–274, doi:10.1016/j.gr.2007.05.003, 2008.

Fountain, A. G., Lewis, K. J. and Doran, P. T.: Spatial climatic variation and its control on glacier equilibrium line altitude in Taylor Valley, Antarctica., 1999.

Fraser, C. I., Nikula, R., Ruzzante, D. E. and Waters, J. M.: Poleward bound: Biological impacts of Southern Hemisphere glaciation, Trends Ecol. Evol., 27(8), 462–471, doi:10.1016/j.tree.2012.04.011, 2012.

Frey, M. M., Savarino, J., Morin, S., Erbland, J. and Martins, J. M. F.: Photolysis imprint in the nitrate stable isotope signal in snow and atmosphere of East Antarctica and implications for reactive nitrogen cycling., 2009.

Gasson, E., DeConto, R. M., Pollard, D. and Levy, R. H.: Dynamic Antarctic ice sheet during the early to mid-Miocene, Proc. Natl. Acad. Sci. U. S. A., 113(13), 3459–3464, doi:10.1073/pnas.1516130113, 2016.

Golledge, N. R., Fogwill, C. J., Mackintosh, A. N. and Buckley, K. M.: Dynamics of the last glacial maximum Antarctic ice-sheet and its response to ocean forcing, Proc. Natl. Acad. Sci. U. S. A., 109(40), 16052–16056, doi:10.1073/pnas.1, 2012.

Golledge, N. R., Levy, R. H., McKay, R. M., Fogwill, C. J., White, D. A., Graham, A. G. C., Smith, J. A., Hillenbrand, C. D., Licht, K. J., Denton, G. H., Ackert, R. P., Maas, S. M. and Hall, B. L.: Glaciology and geological signature of the Last Glacial Maximum Antarctic ice sheet, Quat. Sci. Rev., 78, 225–247, doi:10.1016/j.quascirev.2013.08.011, 2013.

Graham, I., Ditchburn, R. G., Claridge, G. G. G., Whitehead, N. E., Zondervan, A. and Sheppard, D. S.: Dating Antarctic soils using atmospheric derived 10Be and nitrate, R. Soc. New Zeal. Bull., 35, 429–436, 2002.

Graly, J. A., Bierman, P. R., Reusser, L. J. and Pavich, M. J.: Meteoric 10Be in soil profiles - A global meta-analysis, Geochim. Cosmochim. Acta, 74, 6814–6829, doi:10.1016/j.gca.2010.08.036, 2010.

Graly, J. A., Licht, K. J., Druschel, G. K. and Kaplan, M. R.: Polar desert chronologies through quantitative measurements of salt accumulation, Geology, 46(4), 351–354, doi:10.1130/G39650.1, 2018.

Gulick, S. P. S., Shevenell, A. E., Montelli, A., Fernandez, R., Smith, C., Warny, S., Bohaty, S. M., Sjunneskog, C., Leventer, A., Frederick, B. and Blankenship, D. D.: Initiation and long-term instability of the East Antarctic Ice Sheet, Nature, 552(7684), 225–229, doi:10.1038/nature25026, 2017.

Hambrey, M. J., Webb, P. N., Harwood, D. M. and Krissek, L. A.: Neogene glacial record from the Sirius Group of the Shackleton Glacier region, central Transantarctic Mountains, Antarctica, GSA Bull., 115(8), 994–1015, doi:10.1130/B25183.1, 2003.

Ivy-Ochs, S., Schluchter, C., Kubik, P. W., Dittrich-Hannen, B. and Beer, J.: Minimum 10Be exposure ages of early Pliocene for the Table Mountain plateau and the Sirius Group at Mount Fleming, Dry Valleys, Antarctica, Geology, 23(11), 1007–1010, 1995.

Jackson, A., Davila, A. F., Böhlke, J. K., Sturchio, N. C., Sevanthi, R., Estrada, N., Brundrett, M., Lacelle, D., McKay, C. P., Poghosyan, A., Pollard, W. and Zacny, K.: Deposition, accumulation, and alteration of Cl-, NO3-, ClO4- and ClO3- salts in a hyper-arid polar environment: Mass balance and isotopic constraints, Geochim. Cosmochim. Acta, 182, 197–215, doi:10.1016/j.gca.2016.03.012, 2016.

Jones, R. S., Mackintosh, A. N., Norton, K. P., Golledge, N. R., Fogwill, C. J., Kubik, P. W., Christl, M. and Greenwood, S. L.: Rapid Holocene thinning of an East Antarctic outlet glacier driven by marine ice sheet instability, Nat. Commun., 6(8910), 9910, doi:10.1038/ncomms9910, 2015.

Kaplan, M. R., Licht, K. J., Winckler, G., Schaefer, J. M., Bader, N., Mathieson, C., Roberts, M., Kassab, C. M., Schwartz, R. and Graly, J. A.: Middle to Late Pleistocene stability of the central East Antarctic Ice Sheet at the head of Law Glacier, Geology, 45(11), 963–966, doi:10.1130/G39189.1, 2017.

Korschinek, G., Bergmaier, A., Faestermann, T., Gerstmann, U. C., Knie, K., Rugel, G., Wallner, A., Dillmann, I., Dollinger, G., von Gostomski, C. L., Kossert, K., Maiti, M., Poutivtsev, M. and Remmert, A.: A new value for the half-life of 10Be by Heavy-Ion Elastic Recoil Detection and liquid scintillation counting, Nucl. Instruments Methods Phys. Res. Sect. B Beam Interact. with Mater. Atoms, 268(2), 187–191, doi:10.1016/j.nimb.2009.09.020, 2010.

Lancaster, N., Nickling, W. G. and Gillies, J. A.: Sand transport by wind on complex surfaces: Field studies in the McMurdo Dry Valleys, Antarctica, J. Geophys. Res., 115(F3), F03027, doi:10.1029/2009JF001408, 2010.

Lewis, A. R., Marchant, D. R., Ashworth, A. C., Hedenäs, L., Hemming, S. R., Johnson, J. V., Leng, M. J., Machlus, M. L., Newton, A. E., Raine, J. I., Willenbring, J. K., Williams, M. and Wolfe, A. P.: Mid-Miocene cooling and the extinction of tundra in continental Antarctica, Proc. Natl. Acad. Sci. U. S. A., 105(31), 10676–10680, doi:10.1073/pnas.0802501105, 2008.

Lyons, W. B., Deuerling, K., Welch, K. A., Welch, S. A., Michalski, G., Walters, W. W., Nielsen, U., Wall, D. H., Hogg, I. and Adams, B. J.: The Soil Geochemistry in the Beardmore Glacier Region, Antarctica: Implications for Terrestrial Ecosystem History, Sci. Rep., 6, 26189, doi:10.1038/srep26189, 2016.

MacKintosh, A., Golledge, N., Domack, E., Dunbar, R., Leventer, A., White, D., Pollard, D., Deconto, R., Fink, D., Zwartz, D., Gore, D. and Lavoie, C.: Retreat of the East Antarctic ice sheet during the last glacial termination, Nat. Geosci., 4(3), 195–202, doi:10.1038/ngeo1061, 2011.

Mackintosh, A. N., Verleyen, E., O'Brien, P. E., White, D. A., Jones, R. S., McKay, R., Dunbar, R., Gore, D. B., Fink, D., Post, A. L., Miura, H., Leventer, A., Goodwin, I., Hodgson, D. A., Lilly, K., Crosta, X., Golledge, N. R., Wagner, B., Berg, S., van Ommen, T., Zwartz, D., Roberts, S. J., Vyverman, W. and Masse, G.: Retreat history of the East Antarctic Ice Sheet since the Last Glacial Maximum, Quat. Sci. Rev., 100, 10–30, doi:10.1016/j.quascirev.2013.07.024, 2014.

Marchant, D. R., Denton, G. H., Swisher, C. C. and Potter, N.: Late Cenozoic Antarctic paleoclimate reconstructed from volcanic ashes in the Dry Valleys region of southern Victoria Land, Geol. Soc. Am. Bull., 108(2), 181–194, doi:https://doi.org/10.1130/0016-7606(1996)108%3C0181:LCAPRF%3E2.3.CO;2, 1996.

Margerison, H. R., Phillips, W. M., Stuart, F. M. and Sugden, D. E.: Cosmogenic 3He concentrations in ancient flood deposits from the Coombs Hills, northern Dry Valleys, East Antarctica: interpreting exposure ages and erosion rates, Earth Planet. Sci. Lett., 230(1–2), 163–175, doi:10.1016/J.EPSL.2004.11.007, 2005.

McHargue, L. R. and Damon, P. E.: The global beryllium 10 cycle, Rev. Geophys., 29(2), 141–158, doi:10.1029/91RG00072, 1991.

Menzies, J., van der Meer, J. J. M. and Rose, J.: Till-as a glacial "tectomict", its internal architecture, and the development of a "typing" method for till differentiation, Geomorphology, 75, 172–200, doi:10.1016/j.geomorph.2004.02.017, 2006.

Michalski, G., Bockheim, J. G., Kendall, C. and Thiemens, M.: Isotopic composition of Antarctic Dry Valley nitrate: Implications for NOy sources and cycling in Antarctica, Geophys. Res. Lett., 32(13), 1–4, doi:10.1029/2004GL022121, 2005.

Morgan, D., Putkonen, J., Balco, G. and Stone, J.: Quantifying regolith erosion rates with cosmogenic nuclides 10 Be and 26 Al in the McMurdo Dry Valleys, Antarctica, J. Geophys. Res., 115, F03037, doi:10.1029/2009JF001443, 2010.

Nishiizumi, K., Imamura, M., Caffee, M. W., Southon, J. R., Finkel, R. C. and McAninch, J.: Absolute calibration of 10Be AMS standards, Nucl. Instruments Methods Phys. Res. B, 258, 403–413, doi:10.1016/j.nimb.2007.01.297, 2007.

Paulsen, T. S., Encarnación, J. and Grunow, A. M.: Structure and timing of transpressional deformation in the Shackleton Glacier area, Ross orogen, Antarctica, J. Geol. Soc. London., 161(6), 1027–1038, doi:10.1144/0016-764903-040, 2004.

Pavich, M. J., Brown, L., Klein, J. and Middleton, R.: 10Be accumulation in a soil chronosequence, Earth Planet. Sci. Lett., 68, 198–204, doi:10.1016/0012-821X(84)90151-1, 1984.

Pavich, M. J., Brown, L., Harden, J., Klein, J. and Middleton, R.: 10Be distribution in soils from Merced River terraces, California, Geochim. Cosmochim. Acta, 50, 1727–1735, doi:10.1016/0016-7037(86)90134-1, 1986.

Pollard, D. and DeConto, R. M.: Modelling West Antarctic ice sheet growth and collapse through the past five million years, Nature, 458(7236), 329–332, doi:10.1038/nature07809, 2009.

Reich, M. and Bao, H.: Nitrate deposits of the Atacama Desert: A marker of long-term hyperaridity, Elements, 14(4), 251–256, doi:10.2138/gselements.14.4.251, 2018.

Scherer, R. P., DeConto, R. M., Pollard, D. and Alley, R. B.: Windblown Pliocene diatoms and East Antarctic Ice Sheet retreat, Nat. Commun., 7(1), 1–9, doi:10.1038/ncomms12957, 2016.

Schiller, M., Dickinson, W., Ditchburn, R. G., Graham, I. J. and Zondervan, A.: Atmospheric 10 Be in an Antarctic soil: Implications for climate change, J. Geophys. Res., 114(F1), 1–8, doi:10.1029/2008jf001052, 2009.

Spector, P. and Balco, G.: Exposure-age data from across Antarctica reveal mid-Miocene establishment of polar desert climate, Geol. Soc. Am. | Geol., 1, doi:10.1130/G47783.1, 2020.

Spector, P., Stone, J., Cowdery, S. G., Hall, B., Conway, H. and Bromley, G.: Rapid early-Holocene deglaciation in the Ross Sea, Antarctica, Geophys. Res. Lett., 44(15), 7817–7825, doi:10.1002/2017GL074216, 2017.

Steig, E., Stuiver, M. and Polissar, P.: Cosmogenic isotope concentrations at Taylor Dome, Antarctica, Antarct. J. United States, 30, 95–97, 1995.

Stevens, M. I. and Hogg, I. D.: Long-term isolation and recent range expansion from glacial refugia revealed for the endemic springtail Gomphiocephalus hodgsoni from Victoria Land, Antarctica, Mol. Ecol., 12(9), 2357–2369, doi:10.1046/j.1365-294X.2003.01907.x, 2003.

Stone, J.: A rapid fusion method for separation of beryllium-10 from soils and silicates, Geochim. Cosmochim. Acta, 62(3), 555–561, doi:10.1016/S0016-7037(97)00340-2, 1998.

798 Strasky, S., Di Nicola, L., Baroni, C., Salvatore, M. C., Baur, H., Kubik, P. W., Schlüchter, C. and Wieler, R.:
799 Surface exposure ages imply multiple low-amplitude Pleistocene variations in East Antarctic Ice Sheet, Ricker Hills,
800 Victoria Land, Antarct. Sci., 21(1), 59–69, doi:10.1017/S0954102008001478, 2009.

801 Stroeven, A. P., Prentice, M. L. and Kleman, J.: On marine microfossil transport and pathways in Antarctica during
802 the late Neogene: Evidence from the Sirius Group at Mount Fleming, Geology, 24(8), 727–730, doi:10.1130/0091-
803 7613(1996)024<0727:ommtap>2.3.co;2, 1996.

804 Summerfield, M. A., Stuart, F. M., Cockburn, H. A. P., Sugden, D. E., Denton, G. H., Dunai, T. and Marchant, D.
805 R.: Long-term rates of denudation in the Dry Valleys, Transantarctic Mountains, southern Victoria Land, Antarctica
806 based on in-situ-produced cosmogenic 21Ne, Geomorphology, 27(1–2), 113–129, doi:10.1016/S0169-
807 555X(98)00093-2, 1999.

808 Talarico, F. M., McKay, R. M., Powell, R. D., Sandroni, S. and Naish, T.: Late Cenozoic oscillations of Antarctic
809 ice sheets revealed by provenance of basement clasts and grain detrital modes in ANDRILL core AND-1B, Glob.
810 Planet. Change, 96–97, 23–40, doi:10.1016/j.gloplacha.2009.12.002, 2012.

811 Valletta, R. D., Willenbring, J. K., Lewis, A. R., Ashworth, A. C. and Caffee, M.: Extreme decay of meteoric
812 beryllium-10 as a proxy for persistent aridity, Sci. Rep., 5, 17813, doi:10.1038/srep17813, 2015.

813 Webb, P. N. and Harwood, D. M.: Late Cenozoic glacial history of the Ross embayment, Antarctica, Quat. Sci.
814 Rev., 10(2–3), 215–223, doi:10.1016/0277-3791(91)90020-U, 1991.

815 Webb, P. N., Harwood, D. M., McKelvey, B. C., Mercer, J. H. and Stott, L. D.: Cenozoic marine sedimentation and
816 ice-volume variation on the East Antarctic craton, Geology, 12(5), 287–291, doi:10.1130/0091-
817 7613(1984)12<287:cmsaiv>2.0.co;2, 1984.

818 Webb, P. N., Harwood, D. M., Mabin, M. G. C. and McKelvey, B. C.: A marine and terrestrial Sirius Group
819 succession, middle Beardmore Glacier-Queen Alexandra Range, Transantarctic Mountains, Antarctica, Mar.
820 Micropaleontol., 27(1–4), 273–297, doi:10.1016/0377-8398(95)00066-6, 1996.

821 Welch, K. A., Lyons, W. B., Whisner, C., Gardner, C. B., Gooseff, M. N., Mcknight, D. M. and Priscu, J. C.: Spatial
822 variations in the geochemistry of glacial meltwater streams in the Taylor Valley, Antarctica, Antarct. Sci., 22(6),
823 662–672, doi:10.1017/S0954102010000702, 2010.

824 Willenbring, J. K. and von Blanckenburg, F.: Meteoric cosmogenic Beryllium-10 adsorbed to river sediment and
825 soil: Applications for Earth-surface dynamics, Earth-Science Rev., 98(1–2), 105–122,
826 doi:10.1016/j.earscirev.2009.10.008, 2010.

827 You, C. F., Lee, T. and Li, Y. H.: The partition of Be between soil and water, Chem. Geol., 77(2), 105–118,
828 doi:10.1016/0009-2541(89)90136-8, 1989.

829